JBC Papers in Press. Published on December 9, 2016 as Manuscript M116.771592
The latest version is at http://www.jbc.org/cgi/doi/10.1074/jbc.M116.771592

Endosomal Phosphatidylinositol-3-Phosphate Promotes Gephyrin Clustering and GABAergic Neurotransmission at Inhibitory Postsynapses

Theofilos Papadopoulos,[#1] Hong Jun Rhee,[$] Devaraj Subramanian,[§] Foteini Paraskevopoulou,[$+] Rainer Mueller,[§] Carsten Schultz,[§‡] Nils Brose,[$] Jeong-Seop Rhee,[$] and Heinrich Betz[†¶]

[#]Department of Molecular Biology, Center of Biochemistry and Molecular Cell Biology, Universitätsmedizin Göttingen, Humboldtallee 23, 37073 Göttingen, Germany
[$]Department of Molecular Neurobiology, Max Planck Institute of Experimental Medicine, Hermann-Rein-Straße 3, 37075 Göttingen, Germany
[§]European Molecular Biology Laboratory (EMBL), Cell Biology and Biophysics Unit, Meyerhofstraße 1, 69117 Heidelberg, Germany
[‡]Oregon Health and Science University, Department of Physiology & Pharmacology, 3181 SW Sam Jackson Park Rd, Portland, OR 97239-3098, USA
[†]Department of Neurochemistry, Max Planck Institute for Brain Research, Deutschordenstraße 46, 60528 Frankfurt am Main, Germany
[¶]Max Planck Institute of Medical Research, Jahnstraße 29, 69120 Heidelberg, Germany

[+]Current address: NeuroCure Cluster of Excellence, Charité-Universitätsmedizin Berlin, Charitéplatz 1, 10117 Berlin, Germany.

Running title: *PI3P regulates GABAergic postsynapse formation*

To whom correspondence should be addressed: Dr. Theofilos Papadopoulos, Department of Molecular Biology, Center of Biochemistry and Molecular Cell Biology, Universitätsmedizin Göttingen, Humboldtallee 23, 37073 Göttingen, Germany. Phone: +49551 395952; Fax: +49551 395960; E-mail: theofilos.papadopoulos@med.uni-goettingen.de

Keywords: GABA receptor, inositol phospholipid, phosphatidylinositol phosphatase, synapse, vesicles

ABSTRACT

The formation of neuronal synapses and the dynamic regulation of their efficacy depends on the proper assembly of the postsynaptic neurotransmitter receptor apparatus. Receptor recruitment to inhibitory GABAergic postsynapses requires the scaffold protein gephyrin and the guanine nucleotide exchange factor collybistin (Cb)[2]. *In vitro*, the pleckstrin homology (PH) domain of Cb binds phosphoinositides, specifically phosphatidylinositol-3-phosphate (PI3P). However, whether PI3P is required for inhibitory postsynapse formation is currently unknown. Here, we investigated the role of PI3P at developing GABAergic postsynapses by using a membrane-permeant PI3P derivative, time-lapse confocal imaging, electrophysiology, as well as knock-down and overexpression of PI3P-metabolizing enzymes. Our results provide the first *in cellula* evidence that PI3P located at early/sorting endosomes regulates the postsynaptic clustering of gephyrin and $GABA_A$ receptors, and the strength of inhibitory, but not excitatory, postsynapses, in cultured hippocampal neurons. In human embryonic kidney 293 cells, stimulation of gephyrin cluster formation by PI3P depends on Cb. We hence conclude that the endosomal pool of PI3P, generated by the class III phosphatidylinositol 3-kinase (PI3K-C3), is important for the Cb-mediated recruitment of gephyrin and $GABA_A$ receptors to developing inhibitory postsynapses, and thus the formation of postsynaptic membrane specializations.

Phosphoinositides, phosphorylated derivatives of phosphatidylinositol, are critical regulators of intracellular signaling, membrane traffic, and

cell compartmentalization (1-3). The functional roles of phosphoinositide metabolism have been studied in great detail at the presynaptic terminal, where phosphoinositide turnover is of critical importance for synaptic vesicle (SV) recycling and synapse function (4). Little, however, is known about specific roles of phosphoinositides at postsynapses.

Core components of most inhibitory GABAergic postsynapses are $GABA_A$ receptors ($GABA_A$Rs), the cell adhesion protein neuroligin 2 (NL2), the scaffolding protein gephyrin, and the guanine nucleotide exchange factor collybistin (Cb) (5,6). During the formation of many GABAergic synapses, most notably those at neuronal somata, NL2 is thought to activate Cb, which promotes Cb membrane association and the subsequent recruitment of gephyrin and $GABA_A$Rs (7-9). *In vitro* binding studies indicate that the pleckstrin homology (PH) domain of Cb specifically binds phosphatidylinositol-3-phosphate [PI3P; (9-13)], and this interaction is thought to be essential for the anchoring of NL2/gephyrin/Cb complexes at the postsynaptic plasma membrane of synapses that depend on Cb (7,9). The notion that PI3P binding by the PH domain is required for proper Cb function, is supported by the observation that deletion of the PH domain (14), or the substitution therein of two arginine residues that are essential for PI3P binding (9,11), causes a marked reduction in the density of postsynaptic gephyrin clusters in hippocampal neurons. Furthermore, an emerging feature of Cb missense mutations in patients with epilepsy and intellectual disability appears to be impaired PI3P binding (13,15).

PI3P is enriched on early/sorting endosomes (16) and has important roles in membrane trafficking (17,18). In addition, some studies implicate class II phosphatidylinositol 3-kinase (PI3K) isoforms (PI3K-C2 α / β / γ) in the receptor-triggered accumulation of PI3P at the plasma membrane of various cell types (19,20); however, unequivocal evidence for the presence of PI3P at the neuronal plasma membrane is presently lacking. Thus, it remains unclear whether and how PI3P might contribute to the Cb-mediated anchoring of gephyrin scaffolds beneath the postsynaptic membrane, and whether the affinity and specificity of the Cb/PI3P interaction as determined *in vitro* correlate with a defined role of PI3P in the formation of inhibitory postsynapses.

In the present study, we investigated the role of PI3P at developing GABAergic postsynapses in cultured hippocampal neurons by using a membrane-permeant PI3P derivative (21), time-lapse confocal imaging, electrophysiology, as well as knock-down and overexpression of PI3P-metabolizing enzymes. Our results indicate that a PI3P pool associated with early/sorting endosomes is important for the formation of Cb-dependent inhibitory postsynapses. We thereby provide the first demonstration that PI3P is a critical regulator of postsynaptic gephyrin and $GABA_A$R clustering, and that it is involved in the regulation of inhibitory postsynaptic strength in neurons.

RESULTS

PI3P promotes postsynaptic GFP-gephyring clustering−To assess the specific role of PI3P in the Cb-dependent clustering of gephyrin at inhibitory postsynapses, we focused on hippocampal neurons in culture, which receive glutamatergic and GABAergic synaptic inputs and show defects in GABAergic postsynaptic composition and function upon Cb deletion (22). We first aimed to experimentally increase the intracellular PI3P concentration in cultured neurons by applying a membrane-permeable PI3P-acetoxymethyl (AM) ester derivative, its photoactivatable, 'caged' coumarin-PI3P-AM variant, and, as a negative control, its regioisomer PI4P-AM, all of which had previously been validated in HeLa cells (21) and were recently used for studying vesicular trafficking in muscle cells of X-linked centronuclear myopathy patients (23). Previous studies indicate a distribution of both coumarin-caged and uncaged PIP-AM probes into most cellular membranes (21,24). However, in spite of their wide subcellular distribution these probes demonstrated high structural specificity, presumably through their specific interaction with endogenous PIP-binding proteins. For example, it has been shown that PI3P-AM induces early endosome fusion in living cells, and that the resulting fused endosomes were positive for the endogenous early endosome antigen 1 (EEA1) (21), a known marker of early endosomes which interacts specifically with PI3P via its FYVE finger domain (25). In

contrast, compounds of identical chemical composition as PI3P-AM but structurally slightly different, such as PI4P-AM and the enantiomer of PI3P-AM, were unable to induce early endosome fusion (21). In cultured hippocampal neurons, the AM-modified phosphoinositide variants were efficiently accumulated, as demonstrated by adding 50 µM coumarin-PI3P-AM to the culture medium. Neurons incubated with coumarin-PI3P-AM for ~10 min displayed diffuse coumarin fluorescence (Fig. 1*A*), indicating efficient uptake and wide-spread distribution of the PI3P derivative into intracellular membranes.

For quantitative experiments, we transfected cultured hippocampal neurons at DIV9 with GFP-gephyrin, incubated the transfected neurons one day later for 2 h with 50 µM PI3P-AM (or PI4P-AM), or with the vehicle dimethylsulfoxide (DMSO) only, and analyzed the resulting effects on GFP-gephyrin distribution (Fig. 1*B*, *C*). This protocol allowed us to visualize newly synthesized intracellular gephyrin that is *en route* to the plasma membrane at early stages of inhibitory postsynapse formation [from days *in vitro* (DIV) 9 to DIV 10]. Under these conditions, only few dendritic GFP-gephyrin clusters were formed in the transfected neurons prior to treatment, and most GFP-gephyrin was diffusely distributed in the cells and accumulated in larger somatic structures (Fig. 1*B*, left). The subsequent addition of PI3P-AM for 2 h (Fig. 1*B*, left and *C*), but not of PI4P-AM or DMSO only (Fig. 1*C*), led to an increase in the number of dendritic GFP-gephyrin clusters, to a concomitant reduction of the diffuse cytoplasmic GFP-gephyrin fluorescence, and to an apparent redistribution of GFP-gephyrin from the large cytoplasmic structures to numerous smaller clusters (Fig. 1*B*, left). Three-dimensional reconstruction of confocal image stacks and examination of internal structures in the somata of transfected neurons disclosed an enhanced accumulation of GFP-gephyrin fluorescence within both somatic (Fig. 1*B*, YZ plane views) and perisomatic clusters. Quantification of the total numbers of GFP-gephyrin clusters in identified neurons before and after the 2 h treatment indicated an increase by 76.6% in the neurons treated with PI3P-AM, but not in those treated with DMSO or PI4P-AM (Fig. 1*C*; DMSO, 111.8% ± 7.2%, n=10; PI3P-AM, 176.6% ± 15.6%, n=10; PI4P-AM, 97.9% ± 1.6%, n=10). Qualitatively similar effects were also observed with the coumarin-PI3P-AM derivative upon UV-light photoactivation and 1 h incubation (Fig. 1*A*).

To test for PI3P effects on GFP-gephyrin recruitment to developing dendritic and perisomatic inhibitory postsynapses, we performed confocal live-imaging of GFP-gephyrin-transfected neurons prior to compound treatment (Fig. 2*A*-*C*, left), live-imaging of the same neurons upon 2 h treatment with DMSO, PI3P-AM or PI4P-AM, respectively (Fig. 2*A*-*C*, center), and confocal imaging of these neurons after fixation and post-hoc staining for the vesicular inhibitory amino acid transporter (VIAAT), a marker of GABAergic presynapses (Fig. 2*A*-*C*, right). This revealed an ~1.5-fold increase in the average fluorescence intensity of postsynaptic GFP-gephyrin clusters apposed to presynaptic VIAAT puncta in PI3P-AM treated neurons, but not in cells treated with DMSO only or PI4P-AM (Fig. 2*D*; DMSO, 95.9% ± 3.8%, n=70 postsynaptic clusters; PI3P-AM, 150.4% ± 17.9%, n=70 postsynaptic clusters; PI4P-AM, 98.9% ± 5.1%, n=35 postsynaptic clusters). We hence conclude that membrane-permeant PI3P promotes gephyrin clustering at inhibitory postsynaptic sites. Notably, a considerable fraction of the GFP-gephyrin clusters seen after PI3P-AM treatment were not apposed to VIAAT but appeared intracellularly localized (Fig. 2*B*, right). Their rounded structures suggests that these clusters represented vesicle-associated GFP-gephyrin assemblies rather than amorphous intracellular aggregates, as seen upon overexpression in heterologous cells (26,27) or under particular *in vivo* conditions (28).

PI3P increases the strength of GABAergic postsynapses−Previous studies have demonstrated a strong interdependence between gephyrin and major $GABA_AR$ subunits in postsynaptic clustering (29,30). To determine the physiological consequences of the enhanced postsynaptic GFP-gephyrin clustering found after PI3P-AM treatment, we recorded GABAergic miniature inhibitory postsynaptic currents (mIPSCs) and evoked inhibitory postsynaptic currents (eIPSCs) in autaptic cultures of DIV 9-10 GABAergic neurons from striatum. In these cultures, in which isolated

single neurons form synapses with themselves, pre- and postsynaptic effects of PI3P-AM on GABAergic neurotransmission can be distinguished with relative ease (31). Mean mIPSC amplitudes were significantly (by 83.4 %) increased in PI3P-AM treated neurons (61.6 ± 4.7 pA; n=30) as compared to cells treated with DMSO only (33.6 ± 2.3 pA, n=26; Fig. 3*A* and B). In contrast, mIPSC frequences were not significantly different between the two groups (PI3P-AM, 1.3 ± 0.2 Hz, n=30; DMSO, 1.2 ± 0.4 Hz, n=26; Fig. 3*B*). The larger mIPSC amplitudes and the unchanged mIPSC frequencies in PI3P-AM treated neurons indicate an increased number of functional postsynaptic $GABA_A$Rs, which is in line with the increase in postsynaptic GFP-gephyrin clustering observed upon PI3P-AM treatment (Fig. 2*D*). Furthermore, exogenous application of GABA, which activates both synaptic and extrasynaptic $GABA_A$Rs, led to a significant increase of the mean current amplitude (by 82.4 %) in PI3P-AM treated neurons (1.82 ± 0.24 nA; n=33) as compared and normalized to cells treated with DMSO only (1.00 ± 0.1 nA; n=24; Fig. 3*C*).

As PI3P is present in endosomes at presynaptic terminals (32), we tested whether evoked neurotransmitter release is affected in PI3P-AM treated striatal autaptic neurons. While mean mIPSC amplitudes were strongly increased (Fig. 3*A* and *B*), mean eIPSC amplitudes were reduced (by 53%) in PI3P-AM as compared to DMSO treated cells (PI3P-AM, 1.8 ± 0.33 nA, n=30; DMSO, 3.82 ± 0.5 nA, n=26; Fig. 3*D* left and center). Accordingly, the number of SVs released per action potential (AP) (eIPSC charge/mIPSC charge, see Experimental procedures) was strongly reduced after PI3P-AM treatment (PI3P-AM, 42.7 ± 9.6, n=21; DMSO, 242.1 ± 58.58, n=18; Fig. 3*D*, right). In contrast, postsynaptic responses triggered by hypertonic sucrose solution, which causes the release of the readily releasable pool (RRP) of SVs (33,34), were similar between both groups (PI3P-AM, 1.62 ± 0.27 nC, n=30; DMSO, 1.09 ± 0.17 nC, n=26; Fig. 3*E* left and center). Likewise, the numbers of primed synaptic vesicles (PSVs; RRP charge/mIPSC charge) were not significanly different between PI3P-AM and DMSO treated neurons (PI3P-AM, 1245 ± 216, n=21; DMSO, 969 ± 207, n=18; Fig. 3*E*, right). Based on these results, the SV release probability (P_{vr}) in the PI3P-AM treated neurons, calculated either by dividing the charge transfer during AP evoked IPSCs by the RRP charge (Fig. 3*F*, left) or by dividing the number of SVs released per AP by the number of PSVs (Fig. 3*F*, right), was strongly reduced in the presence of PI3P-AM as compared to DMSO treated neurons. Together, our electrophysiological analyses of autaptic GABAergic neurons indicate that mIPSCs and eIPSCs are regulated differentially upon an increase of PI3P in endomembranes, likely due to an increased $GABA_A$R density at the postsynapse and an impairment of SV recycling at the presynaptic terminal.

PI3P increases the size and percentage of endogenous gephyrin and $GABA_A$Rs at inhibitory postsynaptic sites−To study the effects of PI3P-AM during the early stages of inhibitory synapse formation, we immunostained the autaptic striatal neurons for VIAAT as a marker of GABAergic presynapses, and for gephyrin and the α2 subunit of $GABA_A$Rs, which are co-enriched in GABAergic postsynapses (35). After treating the striatal autaptic cultures at DIV 9 for 2 h with DMSO only (Fig. 4*A*, left) or 50 µM PI3P-AM (Fig. 4*A*, right), immunocytochemistry was performed as indicated. At this developmental stage, gephyrin and $GABA_A$R-α2 immunoreactive clusters were distributed at both extrasynaptic and postsynaptic sites, as indicated by their only partial apposition to VIAAT-positive puncta (Fig. 4*B*). PI3P-AM treatment did not significantly change the total number of dendritic VIAAT, gephyrin or $GABA_A$R-α2 clusters, as compared to DMSO only treated neurons (Fig. 4*C*, left; VIAAT: DMSO, 13.25 ± 1.01 puncta/40 µm, n=20; PI3P-AM, 10.9 ± 0.63 puncta/40 µm, n=20; gephyrin: DMSO, 14.3 ± 1.88 clusters/40 µm, n=20; PI3P-AM, 13.35 ± 1.07 clusters/40 µm, n=20; $GABA_A$R-α2: DMSO, 9.7 ± 1.06 clusters/40 µm, n=20; PI3P-AM, 8.8 ± 0.79 clusters/40 µm, n=20). However, the percentages of synaptic gephyrin and $GABA_A$R-α2 clusters colocalizing with VIAAT immunoreactivity were significantly increased upon PI3P-AM treatment, as compared to DMSO only treated cells (Fig. 4*C*, center; synaptic gephyrin: DMSO, 70.71% ± 3.48%, n=20; PI3P-AM, 83.47% ± 2.37%, n=20; synaptic $GABA_A$R-α2: DMSO, 61.15% ± 3.16%, n=20; PI3P-AM, 82.52% ± 2.78%, n=20). Furthermore, the mean sizes of these synaptic

gephyrin and $GABA_AR$-α2 clusters were significantly larger in PI3P-AM treated neurons, as compared to cells treated with DMSO only (Fig. 4*C*, right; gephyrin: DMSO, 0.18 μm^2 ± 0.014 μm^2, n=20; PI3P-AM, 0.26 μm^2 ± 0.021 μm^2, n=20; $GABA_AR$-α2: DMSO, 0.17 μm^2 ± 0.01 μm^2, n=20; PI3P-AM, 0.22 μm^2 ± 0.016 μm^2, n=20). Together, these immunocytochemical results are consistent with the observed increases in mIPSC mean amplitudes and GABA-induced responses seen in PI3P-AM treated striatal autaptic neurons (Fig. 3*B* and *C*) and indicate that PI3P-AM increases the densities and sizes of synaptic gephyrin and $GABA_AR$ clusters.

PI3P-AM treatment substantially reduces evoked excitatory transmission but has no effect on glutamatergic postsynapses−To further test whether the presynaptic changes produced by PI3P-AM treatment of autaptic GABAergic neurons contribute to the observed increase of their postsynaptic strength, we recorded miniature excitatory postsynaptic currents (mEPSCs) and evoked excitatory postsynaptic currents (eEPSCs) from glutaminergic neurons in autaptic DIV 9-11 hippocampal cultures after a 2 h incubation with either DMSO only or 50 µM PI3P-AM. Notably, here the amplitudes and frequences of mEPSCs were not significantly different between these treatments (Fig. 5*A* and *B*; mEPSC amplitudes: DMSO, 22.42 pA ± 1.38 pA, n=15; PI3P-AM, 25.43 pA ± 1.57 pA, n=21; mEPSC frequencies: DMSO, 1.11 Hz ± 0.24 Hz, n=15; PI3P-AM, 1.33 ± 0.18, n=21), indicating that the density of synaptic excitatory glutamate receptors is unchanged in PI3P-AM treated neurons, as compared to DMSO only treated cells. Furthermore, exogenous application of glutamate led to similar responses in both groups (Fig. 5*C*; DMSO normalized, 1.00 nA ± 0.11 nA, n=19; PI3P-AM, 1.02 nA ± 0.10 nA, n=24); thus the total number of surface glutamate receptors (synaptic + extrasynaptic) was not altered upon PI3P-AM treatment. In contrast, exogenous application of GABA resulted in a significantly larger (by 62 %) mean current amplitude in PI3P-AM treated neurons (1.62 ± 0.18 nA; n=24) as compared and normalized to cells treated with DMSO only (1.00 ± 0.07 nA; n=19; Fig. 3*C*). Thus, PI3P specifically increases the density of surface $GABA_ARs$, but not glutamate receptors, in autaptic hippocampal neurons.

In contrast to its lack of an effect on mEPSCs, PI3P-AM treatment abolished eEPSCs recorded from autaptic hippocampal neurons almost completely (Fig. 5*E*). Notably, 65 % of the PI3P-AM treated cells showed no detectable eEPSCs, whereas the remaining cells (9 out of 26 tested) displayed markedly reduced mean eEPSC amplitudes, as compared to DMSO controls (Fig. 5*E*, center; DMSO, 1.95 nA ± 0.38 nA, n=20; PI3P-AM, 0.28 nA ± 0.04, n=9/26). Analysis of the postsynaptic responses triggered by hypertonic sucrose solution indicated that the RRP of SVs were similar between both groups (Fig. 5*F*; DMSO, 0.16 nC ± 0.03 nC, n=17; PI3P-AM, 0.18 nC ± 0.02 nC, n=25). Accordingly, P_{vr} in the PI3P-AM treated neurons, calculated by dividing the charge transfer during AP evoked EPSCs by the RRP charge, was strongly reduced as compared to DMSO treated neurons (Fig. 5*G*; DMSO, 6.14 % ± 0.81 %, n=17; PI3P-AM, 0.54 % ± 0.13 %, n=16/25). Together, these data indicate that the impairment of SV exocytosis seen after PI3P-AM treatment is not caused by or associated with changes in the density of glutamate receptors in the postsynaptic neuron. Together, these electrophysiological analyses of both GABAergic and glutamatergic autaptic neurons demonstrate a specific increase of surface and synaptic $GABA_ARs$, but not glutamate receptors, upon PI3P-AM treatment.

Phosphatidylinositol 3-kinases and phosphatases involved in the regulation of PI3P levels during GABAergic synapse formation−Earlier reports have shown that individual PI3K inhibitors differentially affect the PI3P pools in endosomal and plasma membrane compartments, which indicates that multiple, different enzymes are involved in the generation of PI3P (36,37). Current consensus is that PI3K-C3 is responsible for the production of the constitutive endosomal pool of PI3P at early/sorting endosomes (17), whereas class II PI3K isoforms (PI3K-C2 α / β / γ) are implicated in both the synthesis of $PI3,4P_2$ and the agonist-mediated accumulation of PI3P at the plasma membrane (18-20). Specifically, the α isoform has been demonstrated to preferentially synthesize $PI3,4P_2$ both *in vitro* and at plasma membrane endocytotic pits *in vivo*, a site where $PI3,4P_2$ is required for membrane constriction prior to endocytic vesicle fission (18,38). Of the

three known class II PI3K isoforms, PI3K-C2 α and PI3K-C2 β are expressed in the mammalian brain, whereas PI3K-C2 γ is not (39,40).

To determine which PI3K enzymes might be relevant for the generation of the PI3P pool involved in postsynaptic gephyrin clustering, we conducted miRNA-based knock-down experiments targeting PI3K-C3, PI3K-C2 α, and PI3K-C2 β in dissociated rat hippocampal neurons. Knock-down efficiences of the different miRNAs were determined by Western blotting of lysates of *Rat*2 fibroblasts (ATCC CRL-1764; a fibroblast cell-line of rat origin) stably expressing the corresponding miRNAs or control miRNAs. This led to the identification of miRNAs, which reduced the expression levels of PI3K-C3, PI3K-C2 α, and PI3K-C2 β by about 79%, 83%, and 83%, respectively (Fig. 6*A* and *B*). In order to focus on postsynaptic defects resulting from downregulating the PI3P-specific kinases and to minimize confounding effects of parallel presynaptic changes, we performed Ca_2PO_4-transfections with vectors expressing GFP and a given miRNA at low transfection efficiences (1-2%) and concentrated our immunocytochemical analysis on the sparse morphologically identifiable pyramidal neurons coexpressing GFP and the respective miRNAs. Cultured rat hippocampal neurons were transfected at DIV 4, and the effects of downregulating the corresponding kinases on gephyrin clustering were analyzed at DIV 14. We detected a significant reduction by ~33% in the density of dendritic gephyrin immunoreactive puncta in neurons expressing the miRNA directed against PI3K-C3, but not in neurons expressing the miRNAs directed against PI3K-C2 α or PI3K-C2 β, as compared to neurons transfected with the control miRNA (Fig. 7*A-B*; Cntrl. miRNA, 24.2 ± 1.2 puncta/40 µm dendritic length, n=21; PI3K-C3 miRNA, 16.1 ± 0.8 puncta/40 µm dendritic length, n=22; PI3K-C2 α miRNA, 22.2 ± 1.1 puncta/40 µm dendritic length, n=14; PI3K-C2 β miRNA, 21.6 ± 1.4 puncta/40 µm dendritic length, n=14). Notably, expression of the PI3K-C3 miRNA had no effect on the density of dendritic VIAAT immunoreactive puncta (Fig. 7*C*; Cntrl. miRNA, 17.9 ± 0.7 puncta/40 µm dendritic length, n=13; PI3K-C3 miRNA; 18.0 ± 1.3 puncta/40 µm dendritic length, n=12), indicating that the number of contacting GABAergic presynapses had not changed. EEA1 is a protein containing a FYVE finger domain that binds to PI3P and targets EEA1 to early/sorting endosomes (25). In agreement with the involvement of PI3K-C3 in generating the PI3P-pool localized on early/sorting endosomes, downregulation of PI3K-C3 by miRNA reduced the density of EEA1 immunoreactive puncta in the dendrites (Fig. 7*F*; Cntrl. miRNA, 22.6 ± 1.8 puncta/40 µm dendritic length, n=10; PI3K-C3 miRNA; 11.8 ± 1.7 puncta/40 µm dendritic length, n=10), but not the somata (Fig. 7*E*; Cntrl. miRNA, 18.6 ± 1.2 puncta/100 µm^2, n=10; PI3K-C3 miRNA; 16.3 ± 2.7 puncta/100 µm^2, n=10), of transfected neurons (Fig. 7*D-F*).

To evaluate whether the effects of PI3K-C3 miRNA downregulation can be rescued by exogeneously added PI3P-AM, we transfected hippocampal cultures at DIV 4, e. g. prior to the onset of inhibitory synapse formation, with the PI3K-C3 miRNA or the control miRNA and subsequently treated them at DIV 8 with 50 µM PI3P-AM or DMSO for 2 h prior to fixation and immunocytochemical analysis. Again, the PI3K-C3 miRNA expressing neurons showed a significant reduction by ~54% in the density of dendritic gephyrin clusters neurons, as compared to cells expressing the control miRNA, when treated with DMSO only (Fig. 7*G*, and *H* top/left; Cntrl. miRNA, 6.06 ± 0.71 puncta/40 µm dendritic length, n=16; PI3K-C3 miRNA, 2.76 ± 0.32 puncta/40 µm dendritic length, n=17). Furthermore, we detected an ~37% reduction in the size of dendritic gephyrin clusters in the PI3K-C3 miRNA expressing neurons, as compared to control miRNA expressing cells (Fig. 7*G*, and *H* bottom/left; Cntrl. miRNA, 0.217 µm^2 ± 0.014 µm^2, n=16; PI3K-C3 miRNA, 0.137 µm^2 ± 0.011 µm^2, n=17). In neurons treated for 2 h with PI3P-AM, the difference in endogenous gephyrin cluster densities between PI3K-C3 and control miRNA expressing cells was similar to that observed with DMSO only-treated cells (Fig. 7*G*, and *H* top/right; Cntrl. miRNA, 6.82 ± 0.42 puncta/40 µm dendritic length, n=17; PI3K-C3 miRNA, 3.35 ± 0.61 puncta/40 µm dendritic length, n=17). Similarly, upon PI3P-AM treatment the mean cluster sizes of the gephyrin immunoreactive puncta did not differ significantly between the PI3K-C3 miRNA and

control miRNA expressing neurons but in both cases were larger than upon DMSO treatment (Fig. 7*H* bottom/right; Cntrl. miRNA, 0.286 μm^2 ± 0.022 μm^2, n=17; PI3K-C3 miRNA, 0.231 μm^2 ± 0.019 μm^2, n=17). Thus, consistent with the results obtained from striatal autaptic neurons (Fig. 4), hippocampal neurons also show a significant change in the mean size, but not density, of endogenous gephyrin clusters after a 2 h treatment with PI3P-AM. Furthermore, these findings demonstrate that the comparatively short incubation with PI3P-AM rescues the reduction in mean gephyrin cluster size, but not density, observed upon prolonged PI3K-C3 miRNA expression.

We next wondered whether raising intracellular PI3P levels by overexpression of recombinant PI3K-C3 similarly would result in enhanced gephyrin clustering, as observed upon PI3P-AM treatment. Hence, we expressed the GFP-tagged human orthologue of PI3K-C3, GFP-hVps34, or, as a control, GFP from DIV 7 to DIV 14 in cultured hippocampal neurons and then analyzed the resulting effects on the clustering of endogenous gephyrin by immunostaining. In contrast to the results obtained with a 2 h PI3P-AM treatment, prolonged overexpression of GFP-hVps34 led to significant increases in the density (GFP, 10.9 ± 1.1 puncta/100 μm^2, n=15; GFP-hVps34, 17.1 ± 1.5 puncta/100 μm^2, n=15) and size (GFP, 0.30 ± 0.03 μm^2, n=562 clusters; GFP-hVps34, 0.54 ± 0.08 μm^2, n=851 clusters) of perisomatic, but not dendritic, gephyrin clusters (Fig. 8*A* and *B*). The reasons for the opposing effects on gephyrin perisomatic and dendritic clusters observed upon prolonged hVps34 expression are currently unknown, but might reflect different functions of PI3K-C3 within the cell or differences in the compartmental contents of PI3P-related kinases and phosphatases (see discussion). In either case, these results further confirm that increases in intracellular PI3P levels lead to enhanced gephyrin clustering.

The ability of PI3P to serve dynamic functions in membrane trafficking and protein sorting relies on the tight spatial and temporal control of the kinases and phosphatases involved in its generation and degradation. Members of the myotubularin phosphatase family, MTMs, are the principal PI3P and PI(3,5)P_2 3-phosphatases. Notably, a pool of membrane-associated PI3K-C3 is bound to MTM1, which competes with GTPases for PI3K-C3 binding [for review see (2)]. This indicates a complex interplay of small GTPases, MTMs, and PI3K-C3 in the tuning of endosomal PI3P levels. Furthermore, the activity of certain inositol polyphosphate 5-phosphatases can lead to an enrichment of PI3P in endosomes or at the plasma membrane. For example, ectopic expression of the 72-kDa 5-phosphatase (72-5ptase; also called pharbin) leads to the depletion of PI(3,5)P_2 and the accumulation of PI3P at the plasma membrane, and thereby promotes the plasma membrane translocation of the glucose transporter 4 in adipocytes (41). This 72-5ptase contains a carboxyterminal CAAX motif for membrane targeting.

To investigate the effects of a PI3P/PI(3,5)P_2-specific 3-phosphatase and a PI(3,5)P_2-specific 5-phosphatase in neurons, we overexpressed HA-tagged 72-5ptase and mCherry-tagged MTM1 fused to a C-terminal CAAX-box prenylation sequence for membrane targeting (38) in dissociated rat hippocampal cultures at early stages of inhibitory postsynapse formation for 2 days (DIV 8-DIV 10) and analyzed their effects on endogenous gephyrin clustering. MTM1-CAAX expression led to significant reductions in both perisomatic and dendritic gephyrin cluster densities, as compared to the corresponding values in neurons expressing mCherry alone (Fig. 9*A* and *B-E*; mCherry perisomatic, 7.2 ± 0.9 per 100 μm^2, n=19; mCherry-MTM1-CAAX perisomatic, 3.5 ± 0.5 per 100 μm^2, n=16; mCherry dendritic, 10.4 ± 0.8 per 40 µm, n=32; mCherry-MTM1-CAAX dendritic, 6.8 ± 1.1, n=29). In contrast, overexpression of 72-5ptase did not have any effects on the density of perisomatic and dendritic gephyrin puncta (Fig. 9*B* and *C*), but led to a significant increase in the size of perisomatic (Fig. 9*D*; mCherry, 0.13 ± 0.01 μm^2, n=370 clusters from 19 neurons; HA-72-5ptase, 0.18 ± 0.01 μm^2, n=647 clusters from 30 neurons), but not dendritic (Fig. 9*E*), gephyrin clusters. Together, these results indicate that changes in the total amount of PI3P in neurons caused by overexpresssion of kinases and phosphatases that control PI3P generation and degradation regulate the extent of gephyrin clustering.

The characteristics of synaptic PI3P

pools−Our finding that the downregulation of PI3K-C3, but not of PI3K-C2 α or PI3K-C2 β, causes a significant reduction in gephyrin cluster density on the dendrites of rat hippocampal neurons indicates that the PI3P pool required for gephyrin clustering is located on early/sorting endosomes, because PI3K-C3 is the kinase responsible for the generation of the constitutive PI3P pool on these endosomal compartments (17). To investigate whether gephyrin associates with PI3P-containing membranes during the initial stages of cluster formation, we transfected rat hippocampal neurons for one day (DIV 9-DIV 10) with vectors expressing mRFP-gephyrin and GFP-2xFYVE, a probe consisting of two tandem PI3P-binding FYVE finger domains that binds PI3P specifically and with high affinity *in vitro* and *in vivo* (16). Newly clustered mRFP-gephyrin partially colocalized with GFP-2xFYVE at both extrasynaptic and inhibitory postsynaptic sites (Fig. 10*A*), as indicated by a 25% co-apposition of the two proteins to presynaptic VIAAT puncta (Fig. 10*B*, *C*).

To exclude the possibility that the observed colocalization of mRFP-gephyrin with GFP-2xFYVE results from a random signal-match due to overexpression of the two proteins in dendritic shafts, we performed time-lapse confocal microscopy to monitor the movement of mRFP- and GFP-positive particles over a period of 30 min. This revealed that mRFP-gephyrin clusters remained stable over the observation period, whereas the GFP-2xFYVE fluorescence associated with early/sorting endosomes showed extensive movement, particularly in the dendrites of transfected neurons (Fig. 7*D*, and Movie 1). However, the GFP-2xFYVE puncta that colocalized with mRFP-gephyrin and were apposed to VIAAT-positive presynapses, as indicated by post-hoc staining for VIAAT upon time-lapse imaging and fluoresence intensity plot-analysis (Fig. 10*D*, bottom, and *E*), showed less movement over time as compared to those that were mRFP-gephyrin negative and not apposed to VIAAT (Fig. 10*D*, and Movie 1). Notably, prolonged expression of GFP-2xFYVE in cultured neurons (DIV 4-11) led to a significant reduction of endogenous gephyrin clusters in the dendrites, as compared to neurons expressing GFP alone (Fig. 11*A*, *B*; untransfected, 11.4 ± 0.5 puncta/40 µm dendritic length, n=26; GFP, 10.3 ± 0.5 puncta/40 µm dendritic length, n=26; GFP-2xFYVE, 7.8 ± 0.6 puncta/40 µm dendritic length, n=26). We attribute this to a competitive masking of membrane-associated PI3P by high levels of GFP-2xFYVE (16,42). Together, the results presented above support the view that PI3P is present within endosomal membrane domains that are closely associated with inhibitory postsynapses, and hence are restricted to lateral diffusion.

PI3P-AM induced redistribution of gephyrin depends on Cb−Different lines of evidence suggest that the stimulation of neuronal gephyrin clustering by PI3P-AM involves Cb. First, Cb is the only component of inhibitory postsynapses known to specifically bind this phosphoinositide (10-12,15). Second, Cb deletions and mutations impairing PI3P binding have been demonstrated to impair Cb-dependent gephyrin clustering in cultured neurons (9-11). Third, several collybistin mutations in humans causing X-linked intellectual disability are associated with a loss of, or reduced, PI3P binding capacity (10,13,15). We therefore examined whether the observed effect of PI3P-AM on gephyrin clustering depends on Cb by using human embryonic kidney 293 (HEK 293) cells expressing both GFP-gephyrin and Cb. This heterologous co-expression system was chosen because i) it has proven highly reliable for the identification of proteins that are implicated in gephyrin clustering, including Cb (43), NL2 (7) and its homolog NL4 (44) as well as the Cb-interacting GTPase TC10 (8); and ii), most importantly, it displays a stringent dependence on Cb of gephyrin cluster formation (14,43).

To allow for proper control of GFP-gephyrin expression levels, we generated a HEK 293 cell line [Flp-In T-Rex HEK 293], which inducibly expresses GFP-gephyrin upon addition of tetracycline (TET) to the culture medium (see Experimental procedures). Fig. 12*A,* left, (TET-ON) shows that in this cell line TET-induction led to the formation of large intracellular GFP-gephyrin aggregates, as described previously (43). Co-expression of the constitutively active CbII-splice variant lacking the N-terminal SH3 domain (ΔSH3CbII) redistributed gephyrin into membrane-associated microclusters (Fig. 12*A*, right). This redistribution is due to the ability of ΔSH3CbII to simultaneously bind gephyrin and membrane lipids [e.g. PI3P; (6,9)]. Notably, the

majority of the mammalian Cb isoforms detected *in vivo* contain an inhibitory SH3 domain that renders the protein inactive in this assay, resulting in the preferential accumulation of gephyrin in cytoplasmic aggregates (14,43). In order to examine the effects of PI3P-AM on gephyrin distribution in the absence or presence of SH3 domain containing Cb, we transfected Flp-In T-Rex-GFP-gephyrin HEK 293 cells with Myc-SH3(+)CbII for 10 h prior to a 4 h TET-induction of GFP-gephyrin expression. Subsequently, the cells were treated for an additional 2 h with either DMSO only (Fig. 12*B*, top) or 50 µM PI3P-AM (Fig. 12*B*, bottom), followed by immunocytochemical analysis. In the absence of SH3(+)CbII ("untransfected"), PI3P-AM treatment had no effect on both the density (Fig. 12*D*, left; DMSO, 1.38 ± 0.18 clusters / cell, n=21; PI3P-AM, 1.43 ± 0.14 clusters / cell, n=21) and mean size (Fig. 12*D*, right; DMSO, 0.32 μm^2 ± 0.04 μm^2, n=21; PI3P-AM, 0.37 μm^2 ± 0.04 μm^2, n=21) of GFP-gephyrin clusters, as compared to DMSO only treated cells. In contrast, in the presence of Myc-SH3(+)CbII ("transfected"), PI3P-AM increased significantly the density (Fig. 12*D*, left; DMSO, 3.76 ± 0.89 clusters / cell, n=21; PI3P-AM, 9.38 ± 1.27 clusters / cell, n=21), and correspondingly reduced the mean size (Fig. 12*D*, right; DMSO, 0.25 μm^2 ± 0.04 μm^2, n=21; PI3P-AM, 0.12 μm^2 ± 0.023 μm^2, n=21), of GFP-gephyrin clusters, as compared to controls. These results indicate that in HEK 293 cells i) PI3P-AM alone has no effect the distribution of gephyrin, and ii) Cb is required for the stimulation of gephyrin redistribution into submembranous clusters by this phosphoinositide.

DISCUSSION

The present study provides the first direct demonstration of a key role of PI3P in the regulation of postsynaptic gephyrin clustering and inhibitory synaptic strength in neurons. Specifically, by using cultured hippocampal neurons transiently expressing GFP-gephyrin we show that increasing intracellular PI3P concentrations with the membrane-permeant derivative PI3P-AM suffices to promote the formation of new gephyrin clusters and to increase the gephyrin content of inhibitory postsynapses by enhancing the membrane recruitment of gephyrin from the cytosol and intracellular vesicle-like structures. In autaptic GABAergic neurons derived from the striatum, the increase in postsynaptic gephyrin induced by PI3P-AM correlated with an increase in postsynaptic $GABA_A$Rs, as illustrated by larger mIPSC amplitudes but unaltered mIPSC frequencies, and by significant increases in the number and mean size of synaptic gephyrin and $GABA_A$R clusters. Furthermore, current responses to externally applied GABA were significantly larger, showing that the number of $GABA_A$Rs at the cell surface had increased. A very similar increase in GABA-induced responses was found in autaptic hippocampal glutamatergic neurons upon PI3P-AM treatment. However, here PI3P-AM had no effect on the densities of surface and postsynaptic glutamate receptors, as indicated by the unaltered sizes of glutamate-induced currents and mEPSC amplitudes. Thus, PI3P-AM does not simply enhance plasma membrane incorporation of receptor containing endosomes at postsynaptic sites but specifically upregulates the formation of inhibitory, but not excitatory, postsynapses.

In both GABAergic and glutamatergic autaptic neurons, PI3P-AM treatment resulted in marked decreases in eIPSC and eEPSC amplitudes without altering RRP sizes; this is consistent with a markedly reduced probability of presynaptic neurotransmitter release. Based on these findings, we conclude that PI3P negatively affects the fusion or exocytosis of SVs at both inhibitory and excitatory presynapses. Currently, the reasons for the presynaptic effects of PI3P-AM are not clear, but it is conceivable that higher local PI3P concentrations might compete with and reduce the $PI(4,5)P_2$-regulated binding of Ca^{2+} to synaptotagmins, and thereby inhibit SNARE-dependent synaptic vesicle fusion, as reported previously (45). Further work will be required to elucidate the precise role of PI3P in presynaptic terminals.

Our knock-down experiments targeting different PI3K isoforms in hippocampal neurons indicate an involvement of PI3K-C3, the enzyme that generates the constitutive pool of PI3P on early/sorting endosomes, in postsynaptic gephyrin clustering. In contrast, PI3K-C2 α and PI3K-C2 β, which are involved in both the synthesis of $PI3,4P_2$ (38) and the *de novo* biosynthesis of PI3P at the plasma membrane (19,20,37,46), appear not to be involved in

postsynaptic gephyrin accumulation. These findings lead to the unexpected conclusion that the pool of PI3P on endomembranes, and not PI3P generated at the plasma membrane, is of crucial relevance for postsynaptic Cb-dependent gephyrin clustering. In addition, we consistently found that i) miRNA-mediated downregulation of PI3K-C3 in cultured hippocampal neurons caused an only ~35% reduction in the density of dendritic gephyrin clusters as compared to control cells, ii) a 2h treatment with PI3P-AM rescued the reduction in mean size, but not density, of dendritic gephyrin clusters observed in neurons overexpressing the PI3K-C3 miRNA, and iii) overexpression of hVps34, the human homologue of PI3K-C3, had opposing effects on gephyrin perisomatic and dendritic clusters, compared to a 2 h treatment of the cells with PI3P-AM. Based on these data, one might speculate that PI3P may not be the only signaling lipid involved in the Cb-dependent accumulation of gephyrin at postsynapses. In agreement with this idea, a recent study indicates broader PIP-specificities for the short Cb splice variant, which lacks the N-terminal SH3 domain, than those determined for an open-conformation mutant (W24A/E262A) of the SH3 domain-containing isoform (12). Furthermore, Vps34 has been shown to exist in two complexes in both yeast and mammalian cells, which not only have opposing effects but can potentially negatively regulate one another [for review see (18)]. Finally, phosphoinositide-interconversion by additional kinases or phosphatases present at different subcellular compartments might partially restore the endosomal PI3P pool in the absence of PI3K-C3. In line with the latter interpretation, overexpression of the $PI(3,5)P_2$-specific phosphatase 72-5ptase/pharbin, which is predicted to increase PI3P levels in the transfected neurons, caused a significant increase in the size of perisomatic gephyrin clusters. This result supports the notion of a complex interplay between additional kinases, phosphatases and PI3K-C3 in the tuning of endosomal PI3P levels and gephyrin clustering.

Of note in this context, a comprehensive siRNA screen employing a functional cell-based assay for gephyrin clustering in HeLa cells as a readout identified PI3K-C3 and PI3K-C2γ as candidate kinases involved in the stabilization of GFP-gephyrin clusters (47). In order to examine the involvement of Cb in the enhancement of gephyrin clustering by PI3P-AM, we employed a similar cell-based assay that relied on a HEK 293 cell line, which inducibly expresses GFP-gephyrin upon TET application and thereby allows to investigate the clustering of newly synthesized gephyrin independently of other neuronal proteins. In aggreement with previous reports (9-11,13,15), our results obtained with this heterologous expression system clearly show that PI3P-AM increases gephyrin cluster formation only upon co-expression of Cb.

The importance of early endosomal PI3P pools for gephyrin clustering, which we demonstrate here, extends our understanding of the mechanisms underlying Cb activation and the subsequent nucleation of gephyrin scaffolds (Fig. 13). Our findings support the view that, at least at early stages of synaptogenesis, PI3P-enriched early/sorting endosomes contribute to the membrane recruitment of Cb/gephyrin complexes. Indeed, a significant fraction of 2xFYVE labelled early/sorting endosomes was closely associated with inhibitory postsynapses and apposed to both VIAAT and gephyrin in DIV 10 cultured hippocampal neurons. Further, prolonged overexpression of the 2xFYVE probe significantly reduced the density of gephyrin clusters along dendrites of cultured hippocampal neurons, presumably by masking PI3P on endomembanes. Based on these results, we propose that the interplay between gephyrin- and Cb-interacting proteins and phosphatases is crucial for interconversion of PI3P and thereby the trafficking of Cb/gephyrin complexes towards the plasma membrane, where the latter might be stabilized through interactions with additional proteins, such as NL2 and NL4 (7,9). In line with this idea, a recent report identified a mechanism for phosphoinositide interconversion from PI3P to PI4P at endosomes *en route* to the plasma membrane and showed that this interconversion enables the subsequent recruitment of the exocyst tethering complex (23). Interestingly, the small GTPase TC10, which interacts in its active, GTP-bound state with Cb (8), also binds to one of the components of the exocyst complex, Exo70, and promotes translocation of Exo70 to the plasma membrane (48).

In line with our finding that PI3K-C3 is important for gephyrin clustering at inhibitory

postsynapses, overexpression of hVps34, the human homologue of PI3K-C3, in hippocampal neurons led to significant increases in the density and size of perisomatic gephyrin clusters. Similarly, overexpression of the SH3-domain-deficient Cb isoform, which strongly binds PI3P (9-11), causes increases in the density and size of perisomatic gephyrin clusters (49,50). This indicates that the interaction of Cb and gephyrin with PI3P-containing endosomes is of particular importance for the regulation of the size of perisomatic synapses, which typically produce a stronger inhibitory drive than the smaller synapses localized on dendrites (51). Furthermore, mutations in both, PI3K-C3 and gephyrin, have been implicated in bipolar disorder and schizoprenia (52,53), and both, phosphoinositides and gephyrin, are potential targets for the therapeutic effects of lithium in bipolar disorder (52,54). Thus, our findings also provide a new view on signaling pathways related to neuropsychiatric disorders, linking them to PI3K-C3 function, PI3P generation, and postsynaptic gephyrin clustering.

In summary, the present study identifies PI3P as an efficient regulator of Cb-dependent gephyrin and $GABA_AR$ clustering and indicates the involvement of early/sorting endosomes during the membrane activation process (55) that is required for gephyrin nucleation and scaffold formation at the postsynaptic plasma membrane of developing inhibitory synapses.

EXPERIMENTAL PROCEDURES

Plasmids and oligonucleotide sequences−The GFP-gephyrin and mRFP-gephyrin constructs used have been described previously (56,57). The pEGFP-N1 vector was purchased from Clontech. The GFP-2xFYVE construct was provided by Dr. Marino Zerial (Dresden, Germany), and vectors encoding mCherry-MTM1-CAAX and mCherry alone (38) were provided by Dr. Volker Haucke (Berlin, Germany). A plasmid encoding the myc-tagged 72-5ptase (41) was provided by Dr. Christina A. Mitchell (Victoria, Australia), and the plasmid encoding GFP-hVps34 was provided by Dr. Matthias Wymann (Basel, Switzerland). The pcDNA 6.2-GW/EmGFP and pcDNA 6.2-GW/EmGFP-miR-neg.Cntrl plasmid were included in the BLOCK-iT Pol II miR RNAi Expression Vector Kit (Invitrogen). The neg. Cntrl sequence without 5′overhangs was: 5′-GAAATGTACTGCGCGTGGAGACGTTTTG GCCACTGACTGACGTCTCCACGCAGTACA TTT-3′. The following single-stranded DNA oligonucleotides endoding the pre-miRNAs of PI3K-C3, PI3K-C2 α and PI3K-C2 β used in this study were purchased from Invitrogen, Germany: PI3K-C3: forward, 5′-TGCTGTCA-AGAAGGTACAAAGATCCTGTTTTGGCCA-CTGACTGACAGGATCTTTACCTTCTTGA-3′. Reverse, 5-CCTGTCAAGAAGGTAAAG-ATCCTGTCAGTCAGTGGCCAAAACAGGA TCTTTGTACCTTCTTGAC-3′. PI3K-C2 α : forward, 5′-TGCTGTACAAATGATGGTTC-AAGGTGGTTTTGGCCACTGACTGACCACC TTGACATCATTTGTA-3′. Reverse, 5′-CCTG-TACAAATGATGTCAAGGTGGTCAGTCAG-TGGCCAAAACCACCTTGAACCATCATTTG TAC-3′. PI3K-C2 β : forward: 5′-TGCTG-ATCACAAACCGACTAGGGAAGGTTTTGG-CCACTGACTGACCTTCCCTACGGTTTGTG AT-3′. Reverse, 5′-CCTGATCACAAACCGT-AGGGAAGGTCAGTCAGTGGCCAAAACCT TCCCTAGTCGGTTTGTGATC-3′.

Antibodies−The following primary antibodies were used for immunocytochemistry: Monoclonal mouse anti-Gephyrin (mAb7a, Connex, 1:3,000), polyclonal guinea-pig anti-VIAAT (Synaptic Systems, 1:2,000), polyclonal rabbit anti-VIAAT, affinity purified (131003, Synaptic Systems, 1:500), monoclonal mouse anti-EEA1 (BD Transduction Laboratories, 1:1,000), polyclonal rabbit anti-hemagglutinin (HA) (Zymed Laboratories, Invitrogen, 1:2,000). The polyclonal guinea-pig anti-$GABA_AR$- α 2 subunit antibody (1:1,000) was kindly provided by Dr. Jean-Marc Fritschy (Zurich, Switzerland). The following secondary antibodies were used for immunocytochemistry: Alexa Fluor 488, 555 or 633 goat anti mouse or goat anti rabbit IgG (Invitrogen, 1:2,000). The following primary antibodies were used for Western blotting: Polyclonal rabbit anti-PIK3C3 (PAB12073, Abnova, 1:500), monoclonal mouse anti-PIK3C2A (anti-PI3-Kinase p170, BD Transduction Laboratories, 1:1,000), monoclonal mouse anti-PIK3C2B (Sigma-Aldrich, 1:1,000), monoclonal mouse anti-Actin (clone AC-40, Sigma-Aldrich, 1:2,000), and monoclonal mouse anti- β -Tubulin (clone TUB 2.1, Sigma-Aldrich, 1:2,500). Bound primary antibodies

were visualized on Western blots using horseradish peroxidase (HRP) conjugated AffiniPure goat anti-mouse or goat anti-rabbit IgGs (Jackson ImmunoResearch Laboratories, 1:10,000).

Generation and expression of pre-microRNA (pre-miRNA) constructs−Annealing of single-stranded oligonucleotides (see 'Plasmids and oligonucleotide sequences'), cloning of the double-stranded oligonucleotides into pcDNA^{TM}6.2-GW/EmGFP-miR, and transformation into One Shot TOP10 chemically competent *Escherichia coli* bacteria was performed according to the manufacturer's instructions (BLOCK-iT Pol II miR RNAi Expression Vector Kits, Invitrogen). All plasmids were confirmed by automated DNA sequencing using the EmGFP forward (5´-GGCATGGACGAGCTGTACAA-3´) and the miRNA reverse (5´-CTCTAGATCAACCACT-TTGT-3´) sequencing primers. Knockdown efficiencies were determined by Western blot analysis as described previously (8) and densitometric scanning of the relative band intensities of the proteins of interest in lysates from stable transfectants of Rat2 cells (ATCC CRL-1764; *Rattus norvegicus* fibroblasts) expressing the corresponding miRNAs for PI3K-C3, PI3K-C2α or PI3K-C2β, as compared to the lysates of cells stably expressing the control miRNA. RNAi knock-downs in hippocampal neurons were performed by transfecting the cultures at DIV 4 with the corresponding miRNA plasmids using the CalPhos mammalian transfection kit (Clontech, Takara Bio). After fixation at DIV 14, the cultures were immunostained as described below.

Transfection and immunostaining of hippocampal neurons−Cultures of hippocampal neurons were prepared from embryonic day 18 (E18) rats. Hippocampi were treated with trypsin in HBSS (Gibco, Life Technologies) for 15 min at 37°C and then dissociated by trituration. Cells were plated on poly-L-lysine-coated glass coverslips at a density of 120,000 cells/ml in Neurobasal medium supplemented with B27 (Gibco), Glutamax (Gibco) and Penicillin-Streptomycin (Roche). Neurons were transfected at different DIV, as indicated in the Results part, using the CalPhos^{TM} mammalian transfection kit (Clontech). Immunocytochemistry with the antibodies listed above was performed as described previously (11). Images were collected with an inverse Leica DMIRE2 microscope equipped with a 63x oil-immersion objective and connected to a Leica TCS SP2 AOBS confocal laser scanning setup (Leica Microsystems), or with an AxioImager Z1 equipped with a Zeiss apochromat 63x objective and an Apotome module (Zeiss). Acquired images were processed identically using the ImageJ software package (http://rsb.info.nih.gov/ij). Single channels were recorded using the same standardized threshold levels. Subsequently, a binary image was generated, and immunoreactive puncta were counted automatically by the ImageJ software, as described previously (8,9).

PI3P-AM/PI4P-AM treatment and time-lapse imaging of transfected hippocampal neurons−Neurons were cultured on poly-L-lysine-coated, 35 mm glass bottom ibidi plates (ibidi GmbH) and transfected as described above. The synthesis of caged-PI3P-AM, PI3P-AM, and PI4P-AM has been described previously (21). PIP-AM derivatives were dissolved in DMSO to make a stock solution of 50 mM. To achieve optimal dispersion of the AM-compounds, appropriate amounts of the 50 mM stock solutions or DMSO only were mixed with Pluronic F-127 (Invitrogen) at a 1:0.5 (v/v) ratio, and added to the imaging medium (Neurobasal-A, phenol red free, Invitrogen, Karlsruhe, Germany) to a final concentration of 50 µM of the AM-compounds. The final conentration of DMSO was 0.1%. The neuronal cultures were washed once and kept in imaging medium during the subsequent procedures. Image-stacks of transfected hippocampal neurons were taken with an inverse Leica DMIRE2 microscope equipped with a 63x oil-immersion objective and connected to a Leica TCS SP2 AOBS (acousto-optical beam splitter) confocal laser scanning setup (Leica Microsystems) 10 min prior to treatment. Media were replaced by imaging media containing DMSO/pluronic, 50 µM PI3P-AM/pluronic, or 50 µM PI4P-AM/pluronic, and the cultures were incubated at 37°C in 5% CO_2 for another 2 h. Subsequently, new image-stacks of the same identified neurons were collected, or the cultures were processed directly for immuno-cytochemistry, as described previously (8).

Cultures of hippocampal and striatal autaptic neurons− Microisland cultures of hippocampal

and striatal neurons were prepared and cultured as reported previously (34,58). Briefly, astrocytes for autaptic cultures were obtained from mouse cortices dissected from P0 wild type animals and enzymatically digested for 15 min at 37°C with 0.25% (w/v) trypsin-EDTA (Gibco, Life technologies). Astrocytes were plated in T75 culture flasks in DMEM (Gibco, Life technologies) containing 10% fetal bovine serum (Gibco), penicillin (100 U/ml)/streptomycin (100 µg/ml; Roche), MITO (Becton Dickinson), and grown for 7-10 DIV. Subsequently, astrocytes were trypsinized and plated at a density of ~30,000 cells/well onto 32 mm-diameter glass coverslips, which had been coated with agarose (Sigma-Aldrich) and stamped using a custom-made stamp to generate 200 µm × 200 µm substrate islands with a coating solution containing poly-D-lysine (Sigma-Aldrich), acetic acid, and collagen (BD Biosciences). Hippocampi and striata from P0 mice were isolated and digested for 60 min at 37°C in DMEM containing 25 U/ml papain (Worthington Biomedical Corporation), 0.2 mg/ml cysteine, 1 mM $CaCl_2$, and 0.5 mM EDTA (Sigma-Aldrich). After washing, the dissociated hippocampal and striatal neurons were seeded onto the micro-island plates in pre-warmed Neurobasal Medium (Gibco, Life technologies) supplemented with B27 (Gibco, Life technologies), Glutamax (Gibco, Life technologies) and penicillin (100 U/ml)/streptomycin (100 µg/ml; Roche) at a density of ~4,000 cell/well. The neurons were allowed to differeniate for 9-11 days prior to recording, and only islands containing single neurons were examined.

Electrophysiological recordings on cultured hippocampal and striatal autaptic neurons−Cells were whole-cell voltage-clamped at -70 mV using a MultiClamp 700B amplifier (Axon Instruments, Molecular Devices) under the control of the Clampex program 10.1 (Molecular Devices). All analyses were performed using AxoGraph X version 1.3.1 (AxoGraph Scientific). The cells were recorded between DIV 9 and 11. PSCs were evoked by depolarizing stimuli from -70 mV to 0 mV for 2 ms. The response to triggered release of the RRP was measured after application of 0.5 M hypertonic sucrose solution. The P_{vr} was calculated by dividing the charge transfer during an AP-evoked response through the charge transfer measured during a response to hypertonic sucrose solution (reflecting the apparent RRP). Miniature spontaneus PSCs were recorded in the presence of 300 nM tetrodotoxin. The number of synaptic vesicles of eIPSC and the total number of primed SVs were calculated by dividing the charge transfer of the evoked release and the response to 0.5 M hypertonic sucrose solution, respectively, through the charge transfer of mIPSCs (33,34). Glutamate- and GABA-induced whole-cell currents were recorded after exogenous application of 100 µM glutamate or 3 µM GABA for 1 s, or 3 s, at a holding voltage of -70 mV. Mean amplitudes of responses to exogenously applied glutamate and GABA in PI3P-AM treated neurons were normalized to those of DMSO treated control cells in the same set of experiments. The extracellular solution contained 140 mM NaCl, 2.4 mM KCl, 10 mM Hepes, 10 mM glucose, 4 mM $CaCl_2$, and 4 mM $MgCl_2$ (320 mOsmol/liter), pH 7.3. The patch-pipette solution for recordings on autaptic neurons contained 136 mM KCl, 17.8 mM Hepes, 1 mM EGTA, 4.6 mM $MgCl_2$, 4 mM NaATP, 0.3 mM Na_2GTP, 15 mM creatine phosphate, and 5 U/ml phosphocreatine kinase (315-320 mOsmol/l), pH 7.4. The series resistance was compensated by ~35-60%. All extracellular solutions were applied with a custom-built fast flow system consisting of an array of flow pipes controlled by a stepper motor that allows complete and rapid solution exchange with time constants of ~30 ms. Pressure was on for 20 ms. All chemicals, except for TTX (Tocris Bioscience), were purchased from Sigma-Aldrich.

Generation, transfection and treatment of the Flp-In T-Rex-GFP-gephyrin HEK293 cell line−The Flp-In T-Rex system (Invitrogen) was used to generate a HEK 293 cell line exhibiting TET-inducible expression of GFP-gephyrin. The following components of the Flp-In T-Rex system were purchased from Invitrogen: i) a Flp-In T-Rex HEK 293 cell line (Cat. No: R780-07), containing two independently intergrated plasmids: the pFRT/lacZeo plasmid, which introduces a single FRT site into the genome and stably expresses the *lacZ*-Zeocin fusion gene under the control of the SV40 early promoter, and the pcDNA6/TR plasmid, stably expressing the Tet repressor gene under the control of the constitutive human cytomegalovirus (CMV)

immediate-early enhancer/promoter; ii) the pcDNA5/FRT/TO expression vector for cloning the GFP-gephyrin cDNA (56) into its *Kpn*I/*Not*I sites. This expression vector expresses the gene of interest under the control of TET-regulated hybrid human CMV/$TetO_2$ promoter and contains the hygromycin resistance gene with a FRT site embedded in the 5′ coding region; and iii) the pOG44 plasmid which constitutively expresses the Flp recombinase under the control of the human CMV promoter. Generation of the Flp-In T-Rex-GFP-gephyrin HEK 293 cell line was performed according to the manufacturer's instructions (Flp-In System, Cat. No. K6010-01, Invitrogen). The cells were cultured and maintained in DMEM (Gibco, Life technologies), 10% (v/v) fetal calf serum (Gibco), 50 U/ml penicilin and 50U/ml streptomycin (Roche), 15 µg/ml blasticidin (Invitrogen) and 200 µg/ml hygromycin B (Invitrogen) at 37 °C and 5% CO_2. GFP-gephyrin expression was induced by the addition of 1 µg/ml tetracycline (Invitrogen) to the medium. Under these conditions, further incubation of the cells for 3-4 h was sufficient to induce the expression of GFP-gephyrin. For transfection, cells were plated in 24-well plates on 12 mm cover slips. Sterile cover slips were coated with Poly-L-lysine [Sigma, 0.001 % (w/v), in Dulbecco's PBS, PAA laboratories], for at least 2 h and washed three times with Dulbecco's PBS before plating. Medium was exchanged to DMEM devoid of supplements prior to transfection, at approximately 80 % confluency. For transfections, 100 ng mCherry-empty vector and 100 ng Myc-ΔSH3CbII or MycSH3(+)CbII cDNA were used per well. Cells were transfected using Lipofectamine 2000 (Invitrogen, Karlsruhe, Germany) following the manufacturer's protocol. DMEM containing 10 % (v/v) fetal calf serum and antibiotics were added 2 h after transfection. GFP-gephyrin expression was induced 10 h after transfection by adding 1 µg/ml tetracyclin to the media. After 4 h, the cells were washed once and kept for additional 2 h in imaging medium medium (Neurobasal-A, phenol red free, Invitrogen) containing 50 µM PI3P-AM or DMSO only, as described above (see PI3P-AM treatment of hippocampal neurons). Subsequently, the cells were fixed and stained as described previously (15). Stainings were inspected under an AxioImager Z1 equipped with a Zeiss apochromat 63x objective (Zeiss, Göttingen, Germany). For GFP-gephyrin, exposure times were kept constant at 170 ms. Quantifications were performed using the ImageJ software package (http://rsb.info.nih.gov/ij).

Statistics−Experimental data were evalutated by investigators blind to experimental conditions. Statistical significance was tested using the unpaired, two-tailed Student's t-test. Values represent means ± SEM. Asterisks indicate significant differences (*$P < 0.05$, **$P < 0.01$, ***$P < 0.001$); n.s., no significant difference.

ACKNOWLEDGMENTS

This work was supported by the German Research Foundation (PA 2087/1-3 to T.P.; SFB1190/P10 to N.B.; TRR83 to C.S.). We thank Drs. Volker Haucke (Berlin, Germany), Christina A. Mitchell (Victoria, Australia), Matthias Wymann (Basel, Switzerland), and Marino Zerial (Dresden, Germany) for providing expression vectors, Drs. Ioannis Alexopoulos and Miso Mitkovski for advice regarding time-lapse confocal imaging, and Felicitas Vauk for help with some of the experiments. F. Paraskevopoulou's present address is: NeuroCure Cluster of Excellence, Charité-Universitätsmedizin Berlin, Charitéplatz 1, 10117 Berlin, Germany.

CONFLICT OF INTEREST

The authors declare that they have no conflicts of interest with the content of this article.

AUTHOR CONTRIBUTIONS

T.P. and H.B. designed the experiments. T.P. performed all experiments with the exception of the electrophysiological recordings, which were designed and performed by H.J.R. and J.S.R.. F.P. helped with overexpression of phosphatases, and D.S, R.M and C.S. synthesized the membrane-permeant phosphoinositides PI3P-AM, caged-PI3P-AM and PI4P-AM and provided advice on their use. T.P., N.B. and H.B. wrote the manuscript. All authors critically reviewed the results and approved the final version of the manuscript.

REFERENCES

1. Balla, T. (2013) Phosphoinositides: tiny lipids with giant impact on cell regulation. *Physiol. Rev.* **93**, 1019-1137
2. Raiborg, C., Schink, K. O., and Stenmark, H. (2013) Class III phosphatidylinositol 3-kinase and its catalytic product PtdIns3P in regulation of endocytic membrane traffic. *The FEBS J.* **280**, 2730-2742
3. Roth, M. G. (2004) Phosphoinositides in constitutive membrane traffic. *Physiol. Rev.* **84**, 699-730
4. Wenk, M. R., and De Camilli, P. (2004) Protein-lipid interactions and phosphoinositide metabolism in membrane traffic: insights from vesicle recycling in nerve terminals. *Proc. Natl. Acad. Sci. U.S.A.* **101**, 8262-8269
5. Luscher, B., Fuchs, T., and Kilpatrick, C. L. (2011) $GABA_A$ receptor trafficking-mediated plasticity of inhibitory synapses. *Neuron* **70**, 385-409
6. Papadopoulos, T., and Soykan, T. (2011) The role of collybistin in gephyrin clustering at inhibitory synapses: facts and open questions. *Front. Cell. Neurosci.* **5**, 11
7. Poulopoulos, A., Aramuni, G., Meyer, G., Soykan, T., Hoon, M., Papadopoulos, T., Zhang, M., Paarmann, I., Fuchs, C., Harvey, K., Jedlicka, P., Schwarzacher, S. W., Betz, H., Harvey, R. J., Brose, N., Zhang, W., and Varoqueaux, F. (2009) Neuroligin 2 drives postsynaptic assembly at perisomatic inhibitory synapses through gephyrin and collybistin. *Neuron* **63**, 628-642
8. Mayer, S., Kumar, R., Jaiswal, M., Soykan, T., Ahmadian, M. R., Brose, N., Betz, H., Rhee, J. S., and Papadopoulos, T. (2013) Collybistin activation by GTP-TC10 enhances postsynaptic gephyrin clustering and hippocampal GABAergic neurotransmission. *Proc. Natl. Acad. Sci. U.S.A.* **110**, 20795-20800
9. Soykan, T., Schneeberger, D., Tria, G., Buechner, C., Bader, N., Svergun, D., Tessmer, I., Poulopoulos, A., Papadopoulos, T., Varoqueaux, F., Schindelin, H., and Brose, N. (2014) A conformational switch in collybistin determines the differentiation of inhibitory postsynapses. *EMBO J.* **33**, 2113-2133
10. Kalscheuer, V. M., Musante, L., Fang, C., Hoffmann, K., Fuchs, C., Carta, E., Deas, E., Venkateswarlu, K., Menzel, C., Ullmann, R., Tommerup, N., Dalpra, L., Tzschach, A., Selicorni, A., Luscher, B., Ropers, H. H., Harvey, K., and Harvey, R. J. (2009) A balanced chromosomal translocation disrupting ARHGEF9 is associated with epilepsy, anxiety, aggression, and mental retardation. *Hum. Mutat.* **30**, 61-68
11. Reddy-Alla, S., Schmitt, B., Birkenfeld, J., Eulenburg, V., Dutertre, S., Bohringer, C., Gotz, M., Betz, H., and Papadopoulos, T. (2010) PH-domain-driven targeting of collybistin but not Cdc42 activation is required for synaptic gephyrin clustering. *Eur. J. Neurosci.* **31**, 1173-1184
12. Ludolphs, M., Schneeberger, D., Soykan, T., Schafer, J., Papadopoulos, T., Brose, N., Schindelin, H., and Steinem, C. (2016) Specificity of collybistin-phosphoinositide interactions: impact of the individual protein domains. *J. Biol. Chem.* **291**, 244-254
13. Long, P., May, M. M., James, V. M., Granno, S., Johnson, J. P., Tarpey, P., Stevenson, R. E., Harvey, K., Schwartz, C. E., and Harvey, R. J. (2015) Missense mutation R338W in ARHGEF9 in a family with X-linked intellectual disability with variable macrocephaly and macro-orchidism. *Front. Mol. Neurosci.* **8**, 83
14. Harvey, K., Duguid, I. C., Alldred, M. J., Beatty, S. E., Ward, H., Keep, N. H., Lingenfelter, S. E., Pearce, B. R., Lundgren, J., Owen, M. J., Smart, T. G., Luscher, B., Rees, M. I., and Harvey, R. J. (2004) The GDP-GTP exchange factor collybistin: An essential determinant of neuronal gephyrin clustering. *J. Neurosci.* **24**, 5816-5826
15. Papadopoulos, T., Schemm, R., Grubmuller, H., and Brose, N. (2015) Lipid binding defects and perturbed synaptogenic activity of a Collybistin R290H mutant that causes epilepsy and intellectual disability. *J. Biol. Chem.* **290**, 8256-8270
16. Gillooly, D. J., Morrow, I. C., Lindsay, M., Gould, R., Bryant, N. J., Gaullier, J. M., Parton, R. G., and Stenmark, H. (2000) Localization of phosphatidylinositol 3-phosphate in yeast and mammalian cells. *EMBO J.* **19**, 4577-4588

17. Schu, P. V., Takegawa, K., Fry, M. J., Stack, J. H., Waterfield, M. D., and Emr, S. D. (1993) Phosphatidylinositol 3-kinase encoded by yeast VPS34 gene essential for protein sorting. *Science* **260**, 88-91
18. Marat, A. L., and Haucke, V. (2016) Phosphatidylinositol 3-phosphates-at the interface between cell signalling and membrane traffic. *EMBO J.* **35**, 561-579
19. Brown, R. A., Domin, J., Arcaro, A., Waterfield, M. D., and Shepherd, P. R. (1999) Insulin activates the alpha isoform of class II phosphoinositide 3-kinase. *J. Biol. Chem.* **274**, 14529-14532
20. Ktori, C., Shepherd, P. R., and O'Rourke, L. (2003) TNF-alpha and leptin activate the alpha-isoform of class II phosphoinositide 3-kinase. *Biochem. Biophys. Res. Commun.* **306**, 139-143
21. Subramanian, D., Laketa, V., Muller, R., Tischer, C., Zarbakhsh, S., Pepperkok, R., and Schultz, C. (2010) Activation of membrane-permeant caged PtdIns(3)P induces endosomal fusion in cells. *Nat. Chem. Biol.* **6**, 324-326
22. Papadopoulos, T., Korte, M., Eulenburg, V., Kubota, H., Retiounskaia, M., Harvey, R. J., Harvey, K., O'Sullivan, G. A., Laube, B., Hulsmann, S., Geiger, J. R., and Betz, H. (2007) Impaired GABAergic transmission and altered hippocampal synaptic plasticity in collybistin-deficient mice. *EMBO J.* **26**, 3888-3899
23. Ketel, K., Krauss, M., Nicot, A. S., Puchkov, D., Wieffer, M., Muller, R., Subramanian, D., Schultz, C., Laporte, J., and Haucke, V. (2016) A phosphoinositide conversion mechanism for exit from endosomes. *Nature* **529**, 408-412
24. Mentel, M., Laketa, V., Subramanian, D., Gillandt, H., and Schultz, C. (2011) Photoactivatable and Cell-Membrane-Permeable Phosphatidylinositol 3,4,5-Trisphosphate. *Angew. Chem. Int. Edit.* **50**, 3811-3814
25. Stenmark, H., Aasland, R., Toh, B. H., and D'Arrigo, A. (1996) Endosomal localization of the autoantigen EEA1 is mediated by a zinc-binding FYVE finger. *J. Biol. Chem.* **271**, 24048-24054
26. Meyer, G., Kirsch, J., Betz, H., and Langosch, D. (1995) Identification of a gephyrin binding motif on the glycine receptor beta subunit. *Neuron* **15**, 563-572
27. Kirsch, J., and Betz, H. (1995) The postsynaptic localization of the glycine receptor-associated protein gephyrin is regulated by the cytoskeleton. *J. Neurosci.* **15**, 4148-4156
28. Seitanidou, T., Nicola, M. A., Triller, A., and Korn, H. (1992) Partial glycinergic denervation induces transient changes in the distribution of a glycine receptor-associated protein in a central neuron. *J. Neurosci.* **12**, 116-131
29. Essrich, C., Lorez, M., Benson, J. A., Fritschy, J. M., and Luscher, B. (1998) Postsynaptic clustering of major $GABA_A$ receptor subtypes requires the gamma 2 subunit and gephyrin. *Nat. Neurosci.* **1**, 563-571
30. Kneussel, M., Brandstatter, J. H., Laube, B., Stahl, S., Muller, U., and Betz, H. (1999) Loss of postsynaptic $GABA_A$ receptor clustering in gephyrin-deficient mice. *J. Neurosci.* **19**, 9289-9297
31. Bekkers, J. M., and Stevens, C. F. (1991) Excitatory and inhibitory autaptic currents in isolated hippocampal neurons maintained in cell culture. *Proc. Natl. Acad. Sci. U.S.A.* **88**, 7834-7838
32. Wucherpfennig, T., Wilsch-Brauninger, M., and Gonzalez-Gaitan, M. (2003) Role of Drosophila Rab5 during endosomal trafficking at the synapse and evoked neurotransmitter release. *J. Cell Biol.* **161**, 609-624
33. Rosenmund, C., and Stevens, C. F. (1996) Definition of the readily releasable pool of vesicles at hippocampal synapses. *Neuron* **16**, 1197-1207
34. Jockusch, W. J., Speidel, D., Sigler, A., Sorensen, J. B., Varoqueaux, F., Rhee, J. S., and Brose, N. (2007) CAPS-1 and CAPS-2 are essential synaptic vesicle priming proteins. *Cell* **131**, 796-808
35. Nair, R., Lauks, J., Jung, S., Cooke, N. E., de Wit, H., Brose, N., Kilimann, M. W., Verhage, M., and Rhee, J. (2013) Neurobeachin regulates neurotransmitter receptor trafficking to synapses. *J. Cell Biol.* **200**, 61-80
36. Maffucci, T., Brancaccio, A., Piccolo, E., Stein, R. C., and Falasca, M. (2003) Insulin induces phosphatidylinositol-3-phosphate formation through TC10 activation. *EMBO J.* **22**, 4178-4189

37. Maffucci, T., Cooke, F. T., Foster, F. M., Traer, C. J., Fry, M. J., and Falasca, M. (2005) Class II phosphoinositide 3-kinase defines a novel signaling pathway in cell migration. *J. Cell Biol.* **169**, 789-799
38. Posor, Y., Eichhorn-Gruenig, M., Puchkov, D., Schoneberg, J., Ullrich, A., Lampe, A., Muller, R., Zarbakhsh, S., Gulluni, F., Hirsch, E., Krauss, M., Schultz, C., Schmoranzer, J., Noe, F., and Haucke, V. (2013) Spatiotemporal control of endocytosis by phosphatidylinositol-3,4-bisphosphate. *Nature* **499**, 233-237
39. El Sheikh, S. S., Domin, J., Tomtitchong, P., Abel, P., Stamp, G., and Lalani, E. N. (2003) Topographical expression of class IA and class II phosphoinositide 3-kinase enzymes in normal human tissues is consistent with a role in differentiation. *BMC Clin. Pathol.* **3**, 4
40. Traer, C. J., Foster, F. M., Abraham, S. M., and Fry, M. J. (2006) Are class II phosphoinositide 3-kinases potential targets for anticancer therapies? *Bull. Cancer* **93**, E53-58
41. Kong, A. M., Horan, K. A., Sriratana, A., Bailey, C. G., Collyer, L. J., Nandurkar, H. H., Shisheva, A., Layton, M. J., Rasko, J. E., Rowe, T., and Mitchell, C. A. (2006) Phosphatidylinositol 3-phosphate [PtdIns3P] is generated at the plasma membrane by an inositol polyphosphate 5-phosphatase: endogenous PtdIns3P can promote GLUT4 translocation to the plasma membrane. *Mol. Cell. Biol.* **26**, 6065-6081
42. Petiot, A., Faure, J., Stenmark, H., and Gruenberg, J. (2003) PI3P signaling regulates receptor sorting but not transport in the endosomal pathway. *J. Cell Biol.* **162**, 971-979
43. Kins, S., Betz, H., and Kirsch, J. (2000) Collybistin, a newly identified brain-specific GEF, induces submembrane clustering of gephyrin. *Nat. Neurosci.* **3**, 22-29.
44. Hoon, M., Soykan, T., Falkenburger, B., Hammer, M., Patrizi, A., Schmidt, K. F., Sassoe-Pognetto, M., Lowel, S., Moser, T., Taschenberger, H., Brose, N., and Varoqueaux, F. (2011) Neuroligin-4 is localized to glycinergic postsynapses and regulates inhibition in the retina. *Proc. Natl. Acad. Sci. U.S.A.* **108**, 3053-3058
45. Park, Y., Hernandez, J. M., van den Bogaart, G., Ahmed, S., Holt, M., Riedel, D., and Jahn, R. (2012) Controlling synaptotagmin activity by electrostatic screening. *Nat. Struct. Mol. Biol.* **19**, 991-997
46. Brown, R. A., and Shepherd, P. R. (2001) Growth factor regulation of the novel class II phosphoinositide 3-kinases. *Biochem. Soc. Trans.* **29**, 535-537
47. Wuchter, J., Beuter, S., Treindl, F., Herrmann, T., Zeck, G., Templin, M. F., and Volkmer, H. (2012) A comprehensive small interfering RNA screen identifies signaling pathways required for gephyrin clustering. *J. Neurosci.* **32**, 14821-14834
48. Inoue, M., Chang, L., Hwang, J., Chiang, S. H., and Saltiel, A. R. (2003) The exocyst complex is required for targeting of Glut4 to the plasma membrane by insulin. *Nature* **422**, 629-633
49. Chiou, T. T., Bonhomme, B., Jin, H., Miralles, C. P., Xiao, H., Fu, Z., Harvey, R. J., Harvey, K., Vicini, S., and De Blas, A. L. (2011) Differential regulation of the postsynaptic clustering of gamma-aminobutyric acid type A ($GABA_A$) receptors by collybistin isoforms. *J. Biol. Chem.* **286**, 22456-22468
50. Tyagarajan, S. K., Ghosh, H., Harvey, K., and Fritschy, J. M. (2011) Collybistin splice variants differentially interact with gephyrin and Cdc42 to regulate gephyrin clustering at GABAergic synapses. *J. Cell Sci.* **124**, 2786-2796
51. Brunig, I., Scotti, E., Sidler, C., and Fritschy, J. M. (2002) Intact sorting, targeting, and clustering of gamma-aminobutyric acid A receptor subtypes in hippocampal neurons in vitro. *J. Comp. Neurol.* **443**, 43-55
52. Stopkova, P., Saito, T., Papolos, D. F., Vevera, J., Paclt, I., Zukov, I., Bersson, Y. B., Margolis, B. A., Strous, R. D., and Lachman, H. M. (2004) Identification of PIK3C3 promoter variant associated with bipolar disorder and schizophrenia. *Biol. Psychiatry* **55**, 981-988
53. Lionel, A. C., Vaags, A. K., Sato, D., Gazzellone, M. J., Mitchell, E. B., Chen, H. Y., Costain, G., Walker, S., Egger, G., Thiruvahindrapuram, B., Merico, D., Prasad, A., Anagnostou, E., Fombonne, E., Zwaigenbaum, L., Roberts, W., Szatmari, P., Fernandez, B. A., Georgieva, L., Brzustowicz, L. M., Roetzer, K., Kaschnitz, W., Vincent, J. B., Windpassinger, C., Marshall, C.

R., Trifiletti, R. R., Kirmani, S., Kirov, G., Petek, E., Hodge, J. C., Bassett, A. S., and Scherer, S. W. (2013) Rare exonic deletions implicate the synaptic organizer Gephyrin (GPHN) in risk for autism, schizophrenia and seizures. *Hum. Mol. Gen.* **22**, 2055-2066

54. Tyagarajan, S. K., Ghosh, H., Yevenes, G. E., Nikonenko, I., Ebeling, C., Schwerdel, C., Sidler, C., Zeilhofer, H. U., Gerrits, B., Muller, D., and Fritschy, J. M. (2011) Regulation of GABAergic synapse formation and plasticity by GSK3beta-dependent phosphorylation of gephyrin. *Proc. Natl. Acad. Sci. U.S.A.* **108**, 379-384
55. Kneussel, M., and Betz, H. (2000) Clustering of inhibitory neurotransmitter receptors at developing postsynaptic sites: the membrane activation model. *Trends Neurosci.* **23**, 429-435
56. Fuhrmann, J. C., Kins, S., Rostaing, P., El Far, O., Kirsch, J., Sheng, M., Triller, A., Betz, H., and Kneussel, M. (2002) Gephyrin interacts with Dynein light chains 1 and 2, components of motor protein complexes. *J. Neurosci.* **22**, 5393-5402
57. Maas, C., Tagnaouti, N., Loebrich, S., Behrend, B., Lappe-Siefke, C., and Kneussel, M. (2006) Neuronal cotransport of glycine receptor and the scaffold protein gephyrin. *J. Cell Biol.* **172**, 441-451
58. Burgalossi, A., Jung, S., Man, K. N., Nair, R., Jockusch, W. J., Wojcik, S. M., Brose, N., and Rhee, J. S. (2012) Analysis of neurotransmitter release mechanisms by photolysis of caged Ca^{2+} in an autaptic neuron culture system. *Nat. Protoc.* **7**, 1351-1365
59. Saiepour, L., Fuchs, C., Patrizi, A., Sassoe-Pognetto, M., Harvey, R. J., and Harvey, K. (2010) Complex role of collybistin and gephyrin in $GABA_A$ receptor clustering. *J. Biol. Chem.* **285**, 29623-29631
60. Kittler, J. T., Thomas, P., Tretter, V., Bogdanov, Y. D., Haucke, V., Smart, T. G., and Moss, S. J. (2004) Huntingtin-associated protein 1 regulates inhibitory synaptic transmission by modulating gamma-aminobutyric acid type A receptor membrane trafficking. *Proc. Natl. Acad. Sci. U.S.A.* **101**, 12736-12741

FOOTNOTES

[1] To whom correspondence may be addressed: Phone: +49551 395952; Fax: +49551 395960; E-mail: theofilos.papadopoulos@med.uni-goettingen.de.

[2] The abbreviations used are: 72-5ptase, 72-kDa 5-phosphatase; AM, acetoxymethyl; AP, action potential; Cb, collybistin; DIV, days *in vitro*; DMSO, dimethylsulfoxide; EEA1, early endosome antigen 1; eEPSCs, evoked excitatory postsynaptic currents; eIPSCs, evoked inhibitory postsynaptic currents; $GABA_A$Rs, $GABA_A$ receptors; HEK, human embryonic kidney; mEPSCs, miniature excitatory postsynaptic currents; mIPSCs, miniature inhibitory postsynaptic currents; MTM1, Myotubularin 1; NL2, neuroligin 2; NL4, neuroligin 4; PH, pleckstrin homology; PI3K-C3, class III phosphatidylinositol 3-kinase; PI3P, phosphatidylinositol-3-phosphate; PSVs, primed synaptic vesicles; P_{vr}, vesicle release probability; RRP, readily releasable pool; SV, synaptic vesicle; TET, tetracycline; TTX, tetrodotoxin; VIAAT, vesicular inhibitory amino acid transporter.

FIGURE AND MOVIE LEGENDS

Figure 1. **PI3P-AM induces formation of GFP-gephyrin clusters in dissociated hippocampal neurons.** *A,* Images show cultured hippocampal neurons transfected from DIV 9-DIV 10 with GFP-gephyrin and treated with either DMSO-only, or 50 µM caged PI3P-AM, for 5 min prior to imaging. The caged PI3P-AM carries a photolabile protecting group (7-diethylamino-4-hydrodymethylcoumarin) which masks the D3-phosphate of PI3P. This protective group was removed at 0 min by short UV-light illumination (5 sec, 405 nm), as described previously (21). Note successful cell entry and wide-spread distribution in intracellular membranes of caged PI3P-AM (bottom, left) at this time point. After UV-light illumination, the number of GFP-gephyrin clusters increased in caged-PI3P-AM- (bottom panels, arrowheads), but not DMSO-treated (top panels), neurons over the subsequent 60 min. Scale bars: 10 µm. *B,* 3D-Reconstruction of confocal image stacks and YZ plane views (right panels) of a single rat hippocampal neuron transfected at DIV 9 with a cDNA encoding GFP-gephyrin. At DIV 10, the medium was replaced with imaging medium (see Experimental procedures), and confocal imaging was performed

10 min prior to PI3P-AM treatment (left) and after a 2 h treatment with 50 µM PI3P-AM (right). Yellow lines indicate the positions of the YZ plane views. Note that PI3P-AM leads to a redistribution of GFP-gephyrin aggregates into numerous clusters. Scale bars: 10 µm. ***C,*** Quantifications of the % change in the number of total clusters (synaptic + extrasynaptic) upon treatment as indicated. Bars correspond to values obtained from the analysis of n=10 neurons per condition from N=3 independent experiments.

Figure 2. **PI3P-AM induces postsynaptic clustering of GFP-gephyrin in dissociated hippocampal neurons.** *A-C,* Cultures were transfected at DIV 9 with a cDNA encoding GFP-gephyrin. At DIV 10, the medium was replaced by imaging medium (see Experimental procedures), and confocal images were sampled 10 min prior to DMSO (*A,* left), PI3P-AM (*B,* left) or PI4P-AM (*C,* left) treatment and 2 h after the addition of either DMSO (*A,* center), 50 µM PI3P-AM (*B,* center) or 50 µM PI4P-AM (*C,* center). The same neurons were again imaged after fixation and post-hoc VIAAT staining in order to visualize inhibitory presynaptic terminals (*A-C,* right panels). Arrowheads in the higher magnifications of the boxed areas indicate synaptic sites positive for both GFP-gephyrin and VIAAT. Scale bars: 10 µm. *D,* Quantifications of the % change in fluorescence intensity of postsynaptic GFP-gephyrin clusters upon treatment as indicated. Values are from 70 (PI3P-AM or DMSO-only), or 35 (PI4P-AM), postsynaptic clusters analyzed on 10, or 5, individual neurons, each, from three independent transfection experiments.

Figure 3. **Post- and presynaptic effects of PI3P-AM in autaptic GABAergic striatal neurons.** *A,* Representative mIPSC traces recorded at a holding potential of -70 mV in the presence of 300 nM TTX from autaptic striatal neurons treated with either PI3P-AM (50 µM; green) or DMSO only (control; grey). *B,* Mean mIPSC amplitudes (left) and frequencies (right) in PI3P-AM treated and control neurons. Note the significant increase of mIPSC amplitudes but not frequencies in PI3P-AM-treated neurons, as compared to controls. *C,* Representative traces (left) and normalized responses (right; see Experimental procedures) induced by 3 µM exogenously applied GABA in PI3P-AM treated (green) and control neurons (grey). *D,* Representative traces of AP-evoked IPSCs (left), mean evoked IPSC amplitudes (center) and mean numbers of synaptic vesicles (SVs) released per AP (right) in PI3P-AM treated (green) and control neurons (grey). *E,* Representative responses to the application of hypertonic (0.5 M) sucrose solution (left), mean charge transfer during the response to hypertonic sucrose solution (apparent RRP size; center) and mean numbers of calculated primed SVs (PSVs; right) in PI3P-AM treated (green) and control neurons (grey). Note the significant decrease in the number of SVs per AP, but not in the number of PSVs, in PI3P-AM treated neurons. *F,* Average vesicular release probabilities (P_{vr}), expressed as the percentage of RRP and calculated by dividing the charge transfer during the AP-evoked response by the charge transfer measured during a response to hypertonic sucrose solution (left), or by dividing the number of SVs released during an AP by the number of SVs in the readily releasable vesicle pool (right), in PI3P-AM treated (green) and control (grey) autaptic neurons. Data in *B*, *C*, *D,* center, *E,* center, and *F,* left were obtained from 26 DMSO and 30 PI3P-AM treated neurons in 4-5 independent experiments. Data in *D,* right, *E,* right, and *F,* right were obtained from 18 DMSO and 21 PI3P-AM treated neurons in 3 independent experiments.

Figure 4. **PI3P-AM enhances postsynaptic clustering of gephyrin and $GABA_A$Rs in autaptic GABAergic striatal neurons.** *A-B,* Representative images of autaptic striatal neurons treated at DIV 9 for 2 h with either DMSO only (left), or 50 µM PI3P-AM (right), in imaging medium (see Experimental procedures). Cells were fixed after treatment and stained with gephyrin-, VIAAT- and $GABA_A$R-α2-specific antibodies, as indicated. Scale bars: 10 µm. *B,* Overlays and single channels of the corresponding boxed areas in *A*, at higher magnifications, as indicated. Note increases in the size of synaptically localized gephyrin and, to a lesser extent, α2 subunit-containing $GABA_A$Rs in neurons treated with PI3P-AM, as compared to control cells. *C,* Quantifications of (left) the densities of VIAAT, gephyrin and $GABA_A$R α2 immunoreactive puncta per 40 µm dendritic length, and of (center) the percentages and (right) the mean sizes of synaptically localized dendritic gephyrin and $GABA_A$R α2 clusters in PI3P-AM treated (green) and control (grey) autaptic neurons. Bars correspond to counts on randomly selected dendrites of 20 individual neurons from three independent treatments per condition.

Figure 5. **Post- and presynaptic effects of PI3P-AM in autaptic glutamatergic hippocampal neurons.** *A,* Representative mEPSC traces recorded at a holding potential of -70 mV in the presence of 300 nM TTX from autaptic hippocampal neurons treated with either PI3P-AM (50 µM; blue) or DMSO only (control; grey). *B,* Mean mEPSC amplitudes (left) and frequencies (right) are not significantly different in PI3P-AM treated (blue) and control (grey) neurons. *C,* Representative traces (left) and normalized responses (right; see Experimental procedures) induced by 100 µM exogenously applied glutamate in PI3P-AM treated (blue) and control neurons (grey). *D,* Representative traces (left) and normalized responses (right; see Experimental procedures) induced by 3 µM exogenously applied GABA in PI3P-AM treated (blue) and control neurons (grey). Note that, in contrast to glutamate induced currents, GABA responses are increased in PI3P-AM treated neurons. *E,* Representative traces of AP-evoked EPSCs (left) and mean evoked EPSC amplitudes (right) in PI3P-AM treated (blue) and control neurons (grey). *F,* Representative responses to the application of hypertonic (0.5 M) sucrose solution (left) and mean charge transfer during the response to hypertonic sucrose solution (apparent RRP size; right) in PI3P-AM treated (blue) and control neurons (grey). Note strong decrease in the mean amplitude of the eEPSCs, but not in RRP size, in PI3P-AM treated neurons, as compared to controls. *G,* Average vesicular release probabilities (P_{vr}), expressed as the percentage of RRP and calculated by dividing the charge transfer during the AP-evoked response by the charge transfer measured during a response to hypertonic sucrose solution, in PI3P-AM treated (blue) and control (grey) autaptic hippocampal neurons. Data in *B* were obtained from 15 DMSO and 21 PI3P-AM treated neurons, data in *C* and *D* from 19 DMSO and 24 PI3P-AM treated neurons, and data *E* from 20 DMSO and 9 out of 26 measured PI3P-AM treated neurons, in three independent experiments, each. Data in *F* and *G* are from 17 DMSO and 16 out of 25 analyzed PI3P-AM treated neurons in three independent experiments.

Figure 6. **Downregulation of kinases involved in PI3P-synthesis.** *A,* Western blot analysis of lysates from Rat2 cells stably expressing neg. Cntrl.-miRNA or miRNAs specific for the rat isoforms of PI3K-C3, PI3K-C2 α , or PI3K-C2 β , as indicated. Top panels: Western blotting with antibodies specific for PI3K-C3 (left), PI3K-C2 α (center), or PI3K-C2 β (right). Center panels: A β -tubulin-specific antibody was used to monitor protein loading. Bottom panels: MemCode stainings of the same membranes prior to immunoblotting were used to ensure that similar amounts of total protein were present in the samples analyzed. *B,* Knock-down efficiences were calculated by comparing normalized band intensities (kinase-specific bands normalized to β -tubulin bands) in lysates prepared from cells expressing the neg. Cntrl. miRNA with those from cells expressing the corresponding kinase-specific miRNAs, as indicated. Data represent means ± SEM of 3-4 independent experiments.

Figure 7. **PI3K-C3 knock-down impairs postsynaptic gephyrin clustering.** *A,* Cultured hippocampal neurons were transfected at DIV 4 with a cDNA encoding a GFP-tagged neg. Cntrl.-miRNA (left) or a miRNA specific for rat PI3K-C3 (right). At DIV 14, the cultures were fixed and stained with gephyrin- and VIAAT-specific antibodies. Bottom panels: Overlays of the corresponding boxed areas at higher magnifications. Note the reduction of synaptically localized (as indicated by VIAAT-immunostaining) gephyrin clusters in neurons transfected with the PI3K-C3-specific miRNA. Scale bars: 20 µm. *B,* Quantifications of gephyrin immunoreactive clusters in the dendrites of cultured neurons transfected at DIV 4 with the corresponding miRNAs, as indicated, and analyzed at DIV 14. Bars correspond to counts on randomly selected dendrites of 14-22 individual neurons from three independent transfection experimens. *C,* Quantifications of VIAAT immunoreactive puncta in the dendrites of cultured neurons transfected at DIV 4 with the corresponding miRNAs, as indicated, and analyzed at DIV 14. Bars correspond to counts on randomly selected dendrites of 12-13 individual neurons from three independent transfection experimens. *D,* PI3K-C3 knock-down leads to a reduction of EEA1 immunoreactivity on dendritic early/sorting endosomes. Cultured hippocampal neurons were transfected at DIV 4 either with a cDNA encoding a GFP-tagged neg. Cntrl.-miRNA (top) or a PI3K-C3-specific miRNA (bottom). At DIV 14, the cultures were fixed and stained with an EEA1-specific antibody. Note the reduction of EEA1 immunoreactive punta in the dendrites of neurons expressing the PI3K-C3-miRNA. Scale bars: 10 µm. *E,*

Quantifications of EEA1-immunoreactive puncta in the somata of DIV 14 neurons expressing either the neg. Cntrl. or the PI3K-C3-specific miRNA. Bars correspond to counts on somata (100 µm^2 area) of 10 individual neurons per condition from three independent transfection experimens. *F,* Quantifications of EEA1-immunoreactive puncta in dendritic segments of DIV 14 neurons expressing either the neg. Cntrl. or the PI3K-C3-specific miRNA. Bars correspond to counts on randomly selected dendrites of 10 individual neurons per condition from three independent transfection experimens. *G,* Cultured hippocampal neurons were transfected at DIV 4 with a cDNA encoding the GFP-tagged neg. Cntrl.-miRNA (top panels) or the miRNA specific for rat PI3K-C3 (bottom panels). At DIV 8, the cultures were treated for 2 h either with DMSO only (left) or with 50 µM PI3P-AM (right) in the imaging medium, fixed and stained with a gephyrin-specific antibody. The corresponding boxed areas are shown at higher magnifications. Scale bars: 10 µm. *H,* Quantifications of (top) the densities of gephyrin immunoreactive puncta per 40 µm dendritic length, and (bottom) the mean sizes of dendritic gephyrin clusters, in neg. Cntrl miRNA- (black) and PI3K-C3 miRNA- (green) expressing neurons, treated for 2 h with DMSO or 50 µM PI3P-AM, as indicated. Note increase in the mean size, but not density, of gephyrin clusters in PI3K-C3 miRNA-expressing neurons upon PI3P-AM treatment. Bars correspond to counts on randomly selected dendrites of 16-17 individual neurons from three independent transfections.

Figure 8. **hVPS34 (PI3K-C3) overexpression leads to an increase in the density and size of perisomatic gephyrin clusters in cultured neurons.** *A,* Cultured hippocampal neurons were transfected at DIV 7 with cDNAs encoding either GFP alone (left) or GFP-hVps34 (right). At DIV 14, the cultures were fixed and stained with a gephyrin-specific antibody. Note the increase in perisomatic gephyrin clusters in the neuron expressing GFP-hVps34, as compared to control. Top panels: endogenous gephyrin immunoreactivity; bottom panels: corresponding overlays. Scale bar: 10 µm. *B,* Quantifications of perisomatic (left) and dendritic (right) gephyrin cluster densities and sizes in neurons expressing GFP or GFP-hVps34. Bars correspond to counts on somata (100 µm^2 area) and randomly selected dendrites of 15 individual neurons per condition from three independent transfection experimens.

Figure 9. **Overexpression of MTM1-CAAX or 72-5ptase affects gephyrin clustering in cultured neurons.** *A,* Cultured hippocampal neurons were transfected at DIV 8 with cDNAs encoding either mCherry alone (left), mCherry-MTM1-CAAX (center), or HA-72-5ptase (right). At DIV 10, the cultures were fixed and stained with a gephyrin- (green) and an HA-specific antibody (red in *A,* right). Top panels: endogenous gephyrin immunoreactivity; bottom panels: corresponding overlays. Scale bars: 10 µm. *B-E,* Quantifications of perisomatic and dendritic gephyrin cluster densities (*B, C*) and sizes (*D, E*) in neurons expressing mCherry, mCherry-MTM1-CAAX, or HA-72-5ptase, as indicated. Bars correspond to counts on somata (100 µm^2 area) and randomly selected dendrites (n=29-45) of 16-30 individual neurons per condition from three independent transfection experimens.

Figure 10. **Co-apposition of GFP-2xFYVE and mRFP-gephyrin at inhibitory postsynapses.** *A,* Cultured hippocampal neurons were transfected at DIV 9 with cDNAs encoding GFP-2xFYVE and mRFP-gephyrin. At DIV 10, the cultures were fixed and stained with a VIAAT-specific antibody (blue). Arrows indicate synapses, in which GFP-2xFYVE and mRFP-gephyrin are co-apposed to VIAAT. Scale bar: 10 µm. *B,* Quantifications of mRFP-gephyrin, GFP-2xFYVE, and VIAAT puncta in the dendrites of transfected neurons, as indicated. Bars correspond to counts on randomly selected dendrites of 14 individual neurons collected from three independent transfection experimens. *C,* Percentages of mRFP-gephyrin puncta apposed to 2xFYVE, VIAAT, or co-apposed to both, as indicated. Bars correspond to counts on randomly selected dendrites of 14 individual neurons collected from three independent transfection experimens. *D,* Hippocampal neurons were transfected as in *A*. At DIV 10, time-lapse imaging on a dendritic segment of a neuron expressing GFP-2xFYVE and mRFP-gephyrin was performed. Overlays of the time-points 0 (top) and 30 min (center) are shown. The same dendritic segment was also imaged after fixation and post-hoc VIAAT-staining to visualize inhibitory presynaptic terminals (bottom). Scale bars: 4 µm. *E,* Fluorescence intensity scans over the yellow lines in *D*, illustrating coapposition of GFP-2xFYVE and mRFP-gephyrin with VIAAT during time-lapse imaging.

Black arrowheads in *E* correspond to the white arrowheads in *D* and indicate fluorescence intensity peaks of mRFP-gephyrin and GFP-2xFYVE puncta apposed to VIAAT.

Figure 11. **Prolonged expression of GFP-2xFYVE inhibits clustering of endogenous gephyrin in cultured hippocampal neurons.** *A,* Cultures were transfected at DIV 4 with cDNAs encoding either GFP alone (top) or GFP-2xFYVE (bottom). At DIV 11, neurons were fixed and stained with a gephyrin-specific antibody. Note the reduction in gephyrin cluster density in the neuron expressing GFP-2xFYVE, as compared to the GFP transfected neuron. Left panels: endogenous gephyrin immunoreactivity; right panels: corresponding overlays. Scale bar: 10 µm. *B,* Quantifications of gephyrin clusters per 40 µm dendritic segments in untransfected neurons, neurons expressing GFP, or neurons expressing GFP-2xFYVE. Bars correspond to counts on randomly selected dendrites of 26 individual neurons per condition from three independent transfection experimens.

Figure 12. **In HEK 293 cells, PI3P-AM stimulation of GFP-gephyrin clustering requires Cb.** *A,* Flp-In T-Rex-GFP-gephyrin HEK 293 cells inducibly express GFP-gephyrin upon TET-induction (compare TET-OFF with TET-ON state in the first two panels). Transfection of the Myc-ΔSH3CbII cDNA (unstained) together with empty mCherry vector (in order to allow visualization of transfected cells) resulted in a redistribution of intracellular GFP-gephyrin aggregates into submembranous microclusters (third panel), as reported previously (43). Grayscale panels of the boxed areas displayed at higher magnification (right) demonstrate GFP-gephyrin distributions in the presence (top) or absence (bottom) of ΔSH3CbII. Scale bars: 10 µm. *B,* Flp-In T-Rex-GFP-gephyrin HEK 293 cells were cotransfected in their uninduced state with Myc-SH3(+)CbII and empty mCherry-vector to visualize transfected cells prior to immunocytochemistry. At 10 h post-transfection, GFP-gephyrin expression was induced for 4 h, and then the medium was replaced for 2 h with imaging medium (see Experimental procedures) containing either DMSO only (top panels) or 50 µm PI3P-AM (bottom panels). Subsequently, cells were fixed and stained with a Myc-specific antibody. Grayscale panels of the boxed areas at higher magnifications (right) indicate the redistribution of GFP-gephyrin into numerous smaller clusters in Myc-SH3(+)CbII-expressing cells in the presence of PI3P-AM (bottom), but not DMSO only (top). Scale bars: 10 µm. *C,* Quantifications of the numbers per cell (left) and the mean sizes (right) of GFP-gephyrin clusters in the presence ("transfected") and absence ("untransfected") of Myc-SH3(+)CbII in DMSO- (grey) and PI3P-AM- (green) treated cells. Bars correspond to counts of 21 individual cells per condition from three independent transfections.

Figure 13. **Tentative model for the role of PI3P-containing early/sorting endosomes in the assembly of the gephyrin scaffold at postsynaptic membranes.** *A,* Intracellularly, gephyrin trimers bind to Cb in its closed conformation. At postsynaptic sites, the open conformation is achieved and maintained by the interaction of NL2, NL4 or the α2 subunit of $GABA_A$Rs with the SH3 domain of Cb (7,44,59). In addition, Cb binds in its open conformation, via its PH domain, to PI3P and further PIPs located at the plasma membrane (9,12,15). *B,* Particularly at early developmental stages and at extrasynaptic sites, $GABA_A$Rs undergo constitutive endocytosis and are either rapidly recycled back to the cell surface or targeted to lysosomal degradation (5,60). *C,* Cb [via its SH3 domain (59)] and gephyrin (5) interact with $GABA_A$Rs also at extrasynaptic sites, thereby limiting their diffusion and facilitating their "trapping" to postsynaptic sites. *D,* At $GABA_A$R-containing early/sorting endosomes, both interactions of gephyrin and Cb with $GABA_A$Rs, as well as binding of Cb's PH domain to PI3P, induce the open-conformational state of Cb, thereby increasing the rates of incorporation of receptor-associated scaffold to extrasynaptic or postsynaptic sites. At this stage, levels of gephyrin- and Cb-interacting proteins as well as of PI3K-C3 and additional kinases/phosphatases involved in the generation/degradation of PI3P might be crucial for determining PI3P levels and its interconversion rates and thereby the trafficking of Cb/gephyrin complexes towards the plasma membrane, where the latter might be stabilized through interactions with NL2 and NL4 (see text).

Movie 1. **GFP-2xFYVE colocalizes with stationary mRFP-gephyrin clusters in transfected hippocampal neurons.** *Left*, Time-lapse imaging of a cultured neuron coexpressing GFP-2xFYVE (green) and mRFP-gephyrin (red). *Right*, Single channels of the corresponding boxed area in the overview at higher magnification. Arrowhead indicates a gephyrin cluster with colocalization of GFP-2xFYVE over the observation period of 30 min. Transfection was performed at DIV 9, and time-lapse imaging at DIV 10, as described under Experimental procedures. Time is indicated in the bottom right corner. Scale bars: Left, 10 µm; right, 4 µm.

FIGURE 1

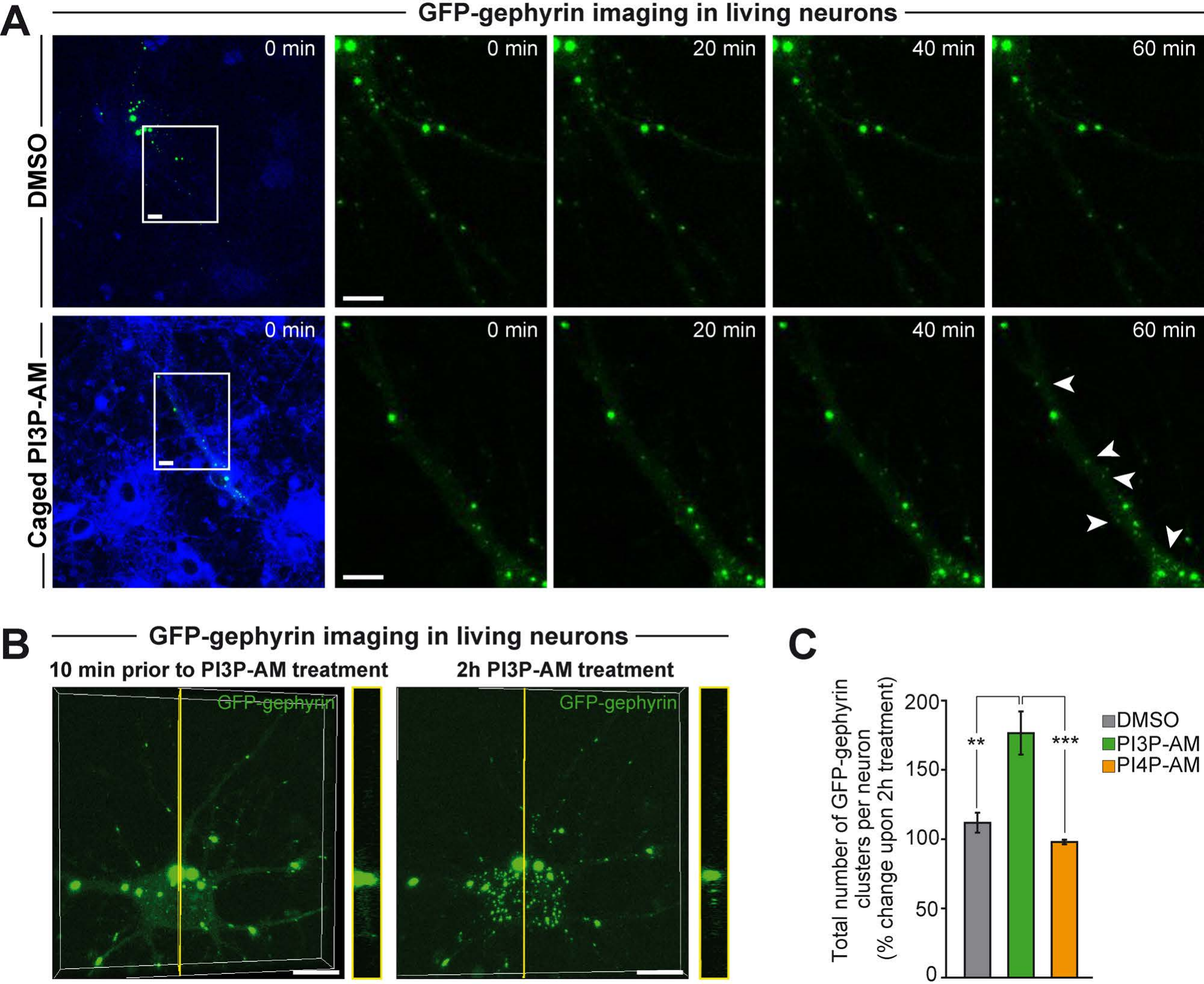
A
GFP-gephyrin imaging in living neurons
DMSO
Caged PI3P-AM
0 min
0 min
20 min
40 min
60 min
0 min
0 min
20 min
40 min
60 min
B
GFP-gephyrin imaging in living neurons
10 min prior to PI3P-AM treatment
2h PI3P-AM treatment
GFP-gephyrin
GFP-gephyrin
C
Total number of GFP-gephyrin clusters per neuron (% change upon 2h treatment)
200
150
100
50
0
**
***
DMSO
PI3P-AM
PI4P-AM

FIGURE 2

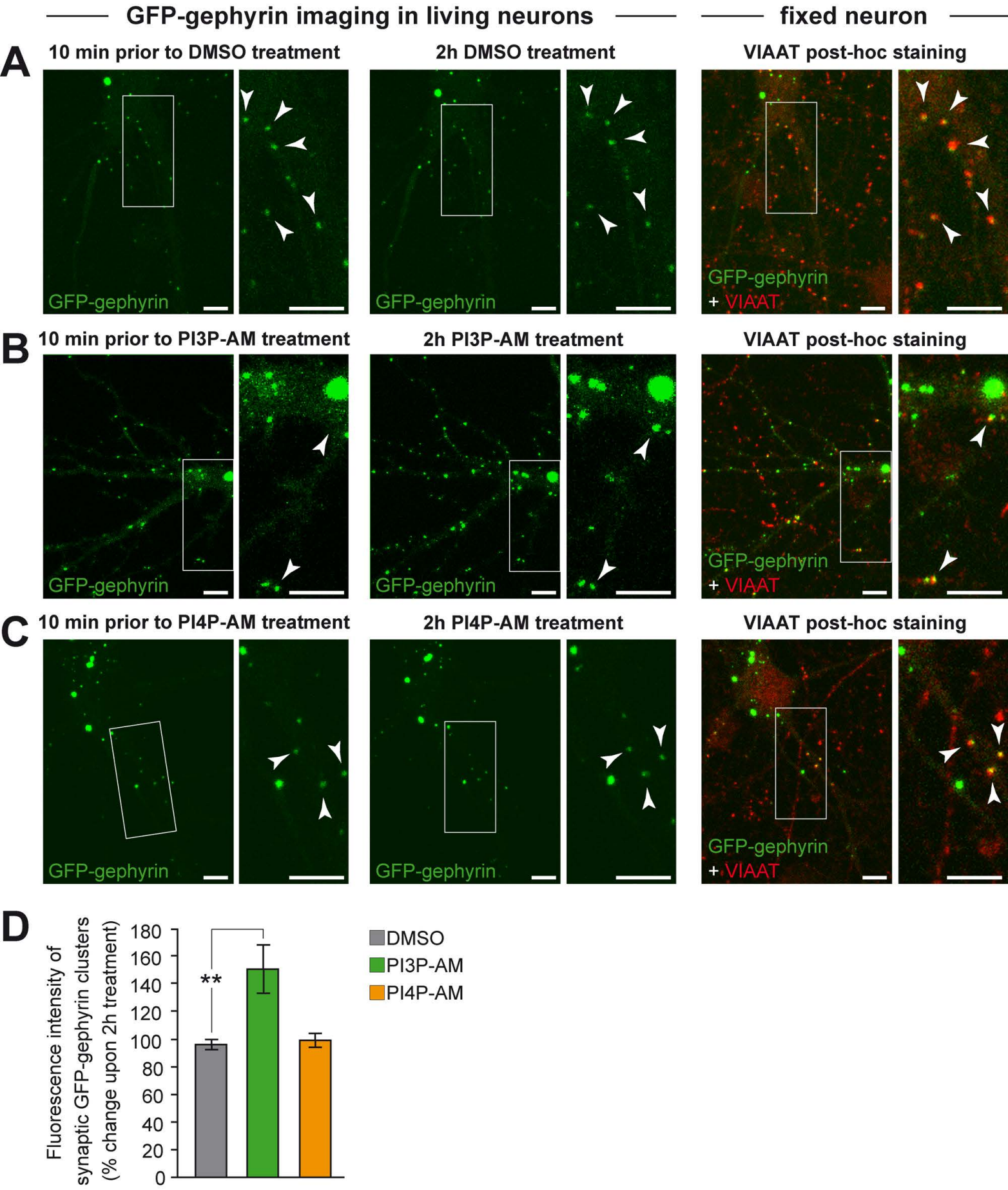
GFP-gephyrin imaging in living neurons
fixed neuron
A
10 min prior to DMSO treatment
2h DMSO treatment
VIAAT post-hoc staining
GFP-gephyrin
GFP-gephyrin
GFP-gephyrin
+ VIAAT
B
10 min prior to PI3P-AM treatment
2h PI3P-AM treatment
VIAAT post-hoc staining
GFP-gephyrin
GFP-gephyrin
GFP-gephyrin
+ VIAAT
C
10 min prior to PI4P-AM treatment
2h PI4P-AM treatment
VIAAT post-hoc staining
GFP-gephyrin
GFP-gephyrin
GFP-gephyrin
+ VIAAT
D
Fluorescence intensity of synaptic GFP-gephyrin clusters (% change upon 2h treatment)
180
160
140
120
100
80
60
40
20
0
**
DMSO
PI3P-AM
PI4P-AM

FIGURE 3

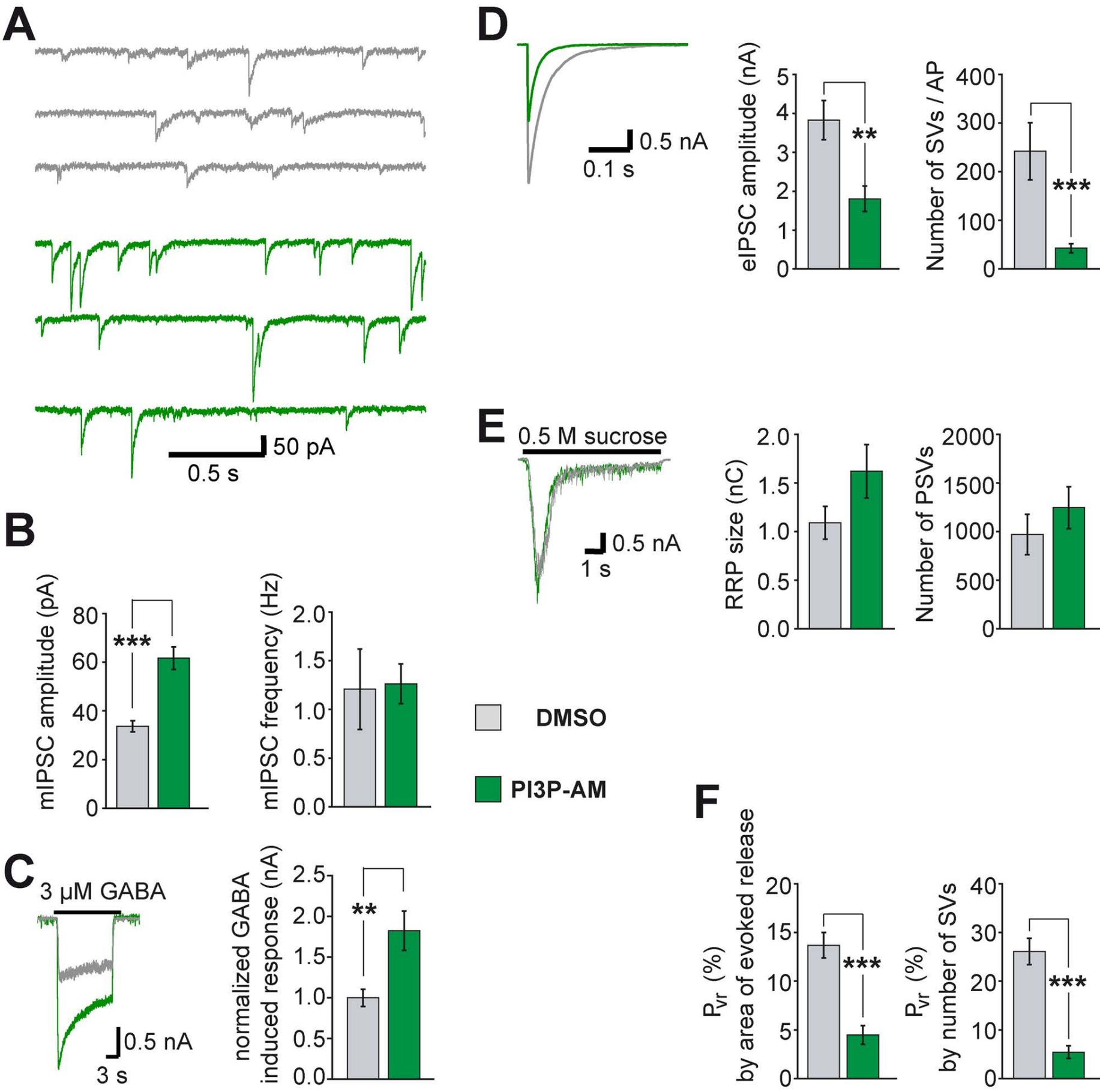
A
50 pA
0.5 s
B
mIPSC amplitude (pA)
***
mIPSC frequency (Hz)
C
3 µM GABA
0.5 nA
3 s
normalized GABA induced response (nA)
**
D
0.5 nA
0.1 s
eIPSC amplitude (nA)
**
Number of SVs / AP
***
E
0.5 M sucrose
0.5 nA
1 s
RRP size (nC)
Number of PSVs
DMSO
PI3P-AM
F
P_vr (%) by area of evoked release
***
P_vr (%) by number of SVs
***

FIGURE 4

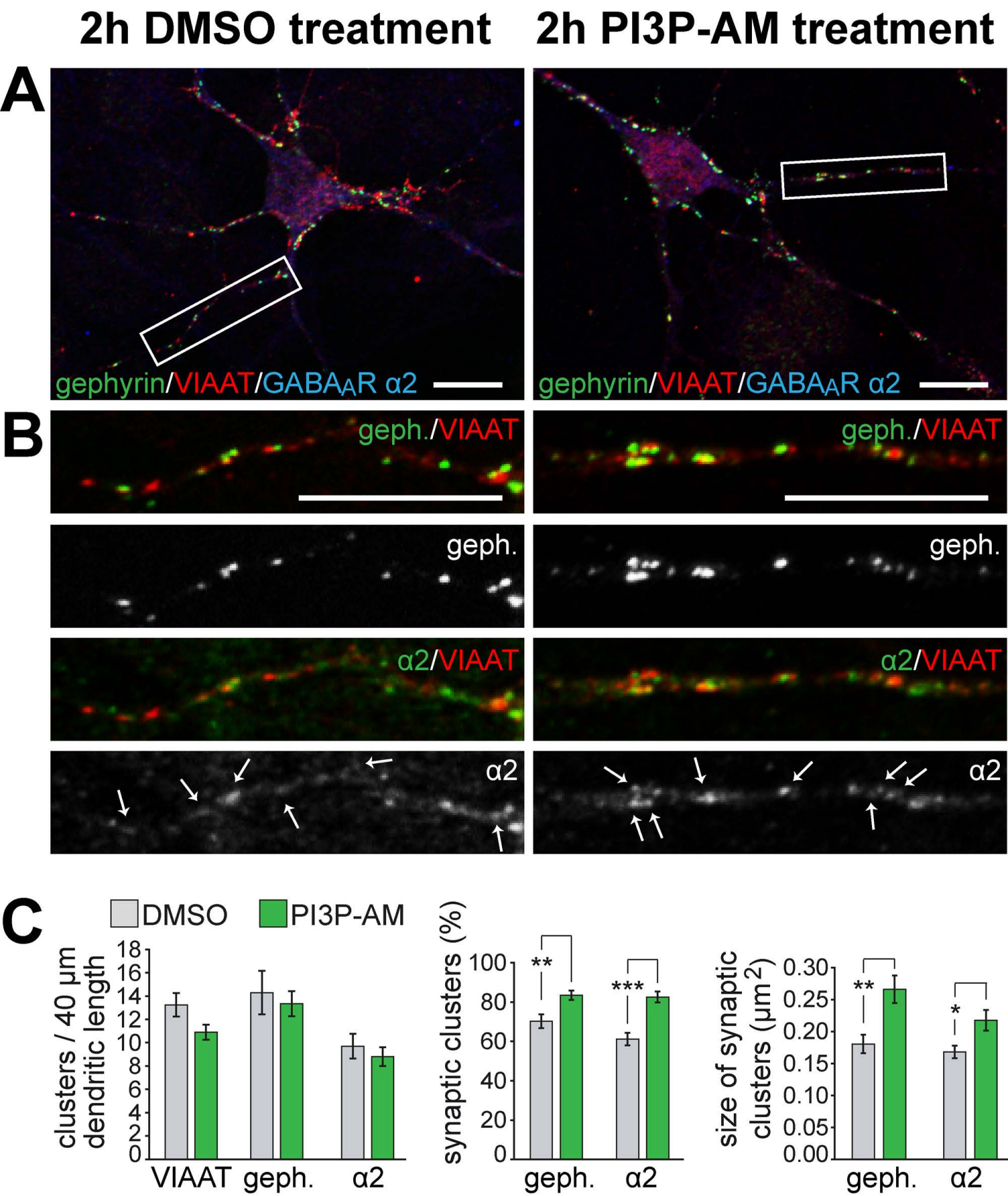
2h DMSO treatment
2h PI3P-AM treatment
A
gephyrin/VIAAT/GABA$_A$R α2
gephyrin/VIAAT/GABA$_A$R α2
B
geph./VIAAT
geph./VIAAT
geph.
geph.
α2/VIAAT
α2/VIAAT
α2
α2
C
DMSO
PI3P-AM
clusters / 40 µm dendritic length
VIAAT
geph.
α2
synaptic clusters (%)
**
***
geph.
α2
size of synaptic clusters (µm^2)
**
*
geph.
α2

FIGURE 5

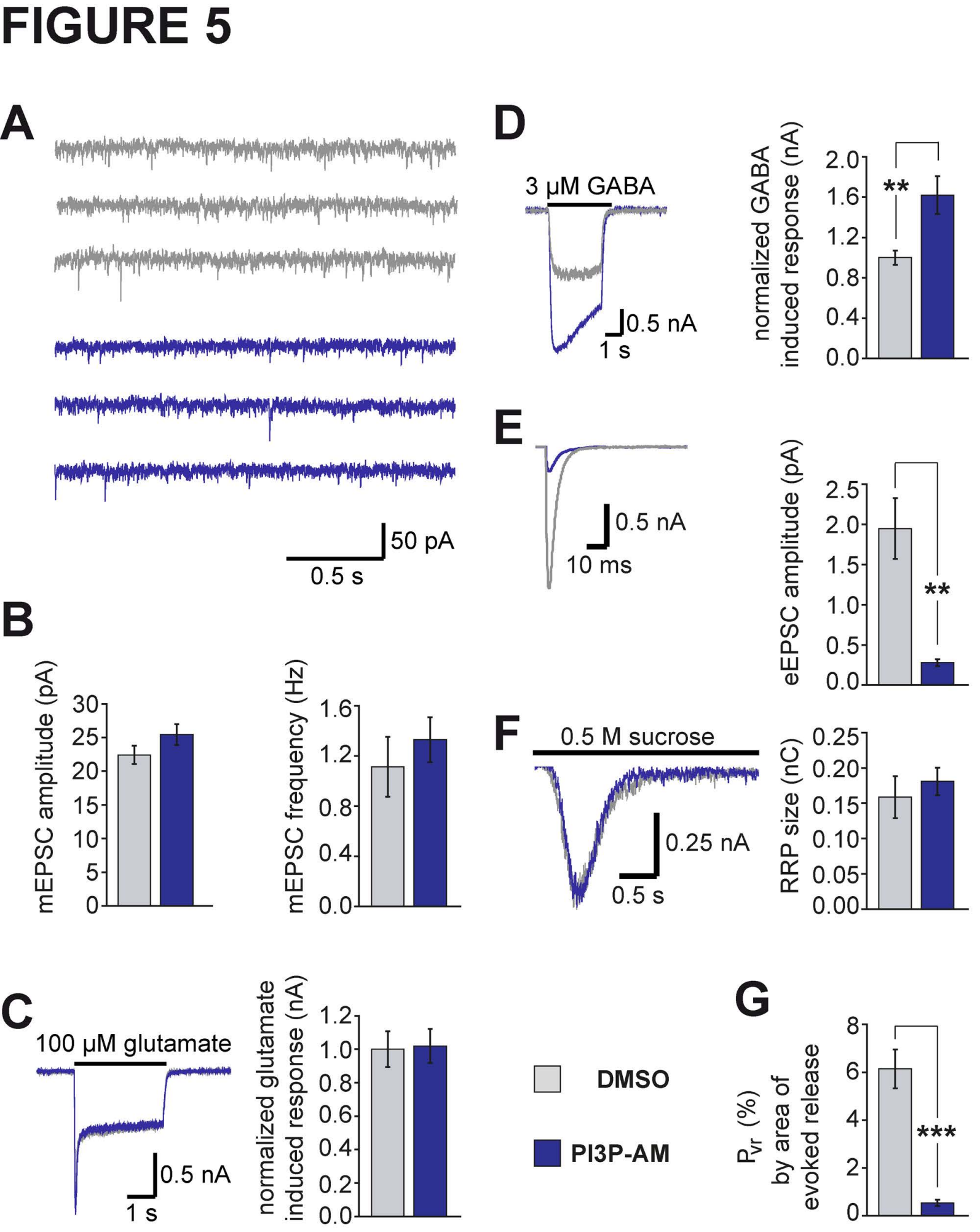
A
50 pA
0.5 s
B
mEPSC amplitude (pA)
30
25
20
15
10
5
0
mEPSC frequency (Hz)
1.6
1.2
0.8
0.4
0.0
C
100 μM glutamate
0.5 nA
1 s
normalized glutamate induced response (nA)
1.2
1.0
0.8
0.6
0.4
0.2
0.0
DMSO
PI3P-AM
D
3 μM GABA
0.5 nA
1 s
normalized GABA induced response (nA)
2.0
1.6
1.2
0.8
0.4
0.0
**
E
0.5 nA
10 ms
eEPSC amplitude (pA)
2.5
2.0
1.5
1.0
0.5
0.0
**
F
0.5 M sucrose
0.25 nA
0.5 s
RRP size (nC)
0.25
0.20
0.15
0.10
0.05
0.00
G
P_{vr} (%) by area of evoked release
8
6
4
2
0
***

FIGURE 6

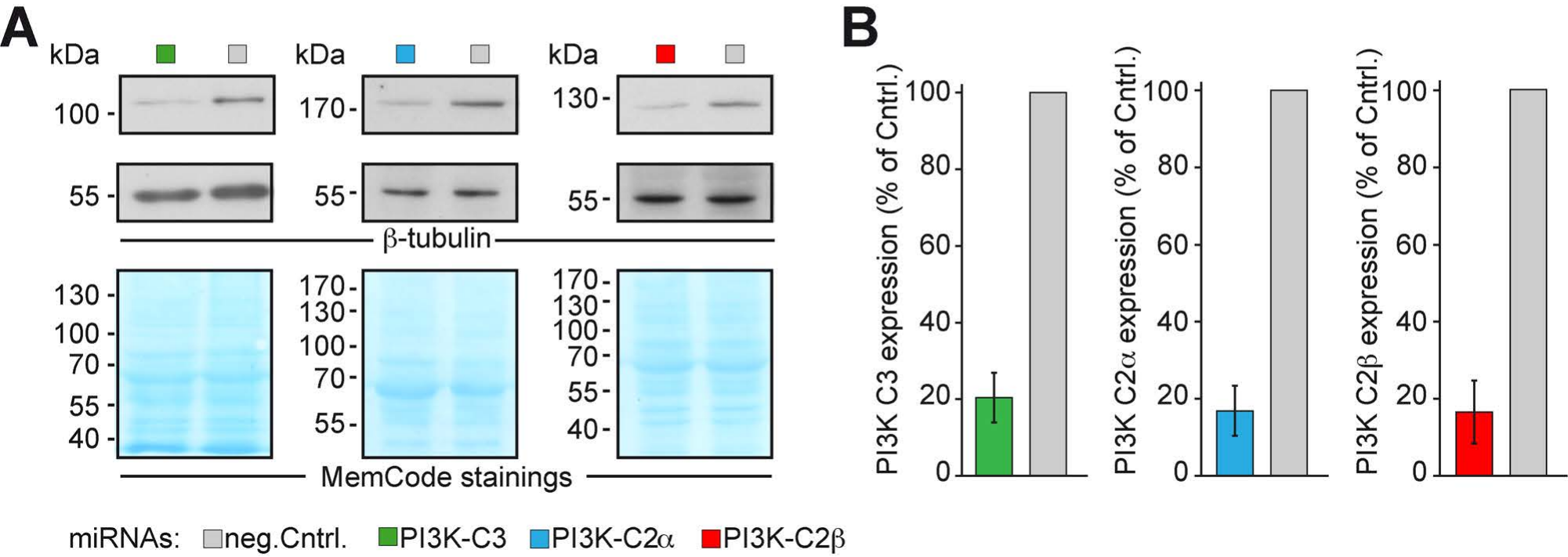
A
kDa
100
55
170
130
β-tubulin
130
100
70
55
40
MemCode stainings
miRNAs: neg.Cntrl. PI3K-C3 PI3K-C2α PI3K-C2β
B
PI3K C3 expression (% of Cntrl.)
PI3K C2α expression (% of Cntrl.)
PI3K C2β expression (% of Cntrl.)
0
20
40
60
80
100

FIGURE 7

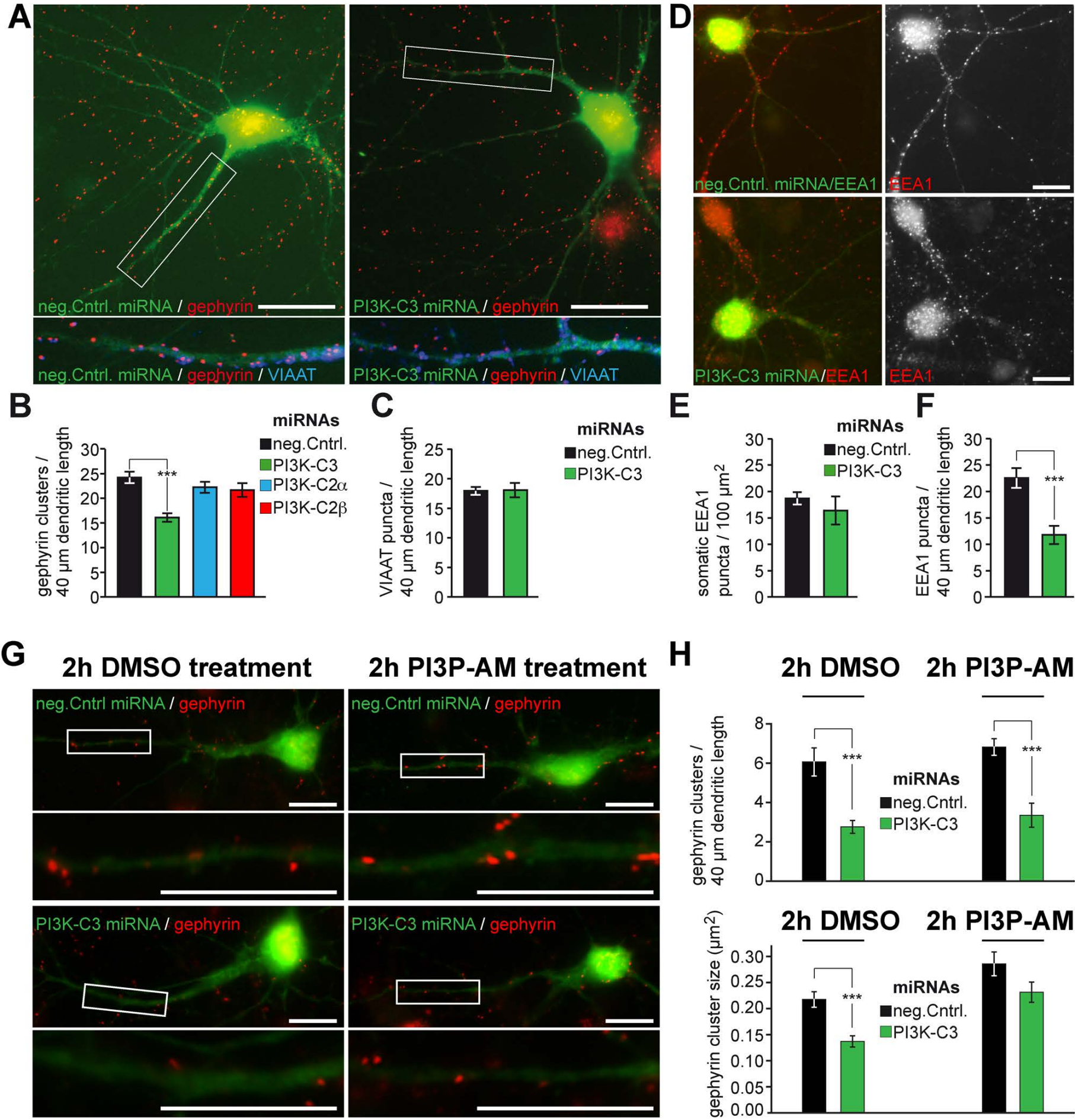
A
neg.Cntrl. miRNA / gephyrin
PI3K-C3 miRNA / gephyrin
neg.Cntrl. miRNA / gephyrin / VIAAT
PI3K-C3 miRNA / gephyrin / VIAAT
D
neg.Cntrl. miRNA/EEA1
EEA1
PI3K-C3 miRNA/EEA1
EEA1
B
gephyrin clusters / 40 µm dendritic length
miRNAs
neg.Cntrl.
PI3K-C3
PI3K-C2α
PI3K-C2β
***
C
VIAAT puncta / 40 µm dendritic length
miRNAs
neg.Cntrl.
PI3K-C3
E
somatic EEA1 puncta / 100 µm²
miRNAs
neg.Cntrl.
PI3K-C3
F
EEA1 puncta / 40 µm dendritic length
***
G
2h DMSO treatment
2h PI3P-AM treatment
neg.Cntrl miRNA / gephyrin
neg.Cntrl miRNA / gephyrin
PI3K-C3 miRNA / gephyrin
PI3K-C3 miRNA / gephyrin
H
2h DMSO
2h PI3P-AM
gephyrin clusters / 40 µm dendritic length
***
***
miRNAs
neg.Cntrl.
PI3K-C3
2h DMSO
2h PI3P-AM
gephyrin cluster size (µm²)
***
miRNAs
neg.Cntrl.
PI3K-C3

FIGURE 8

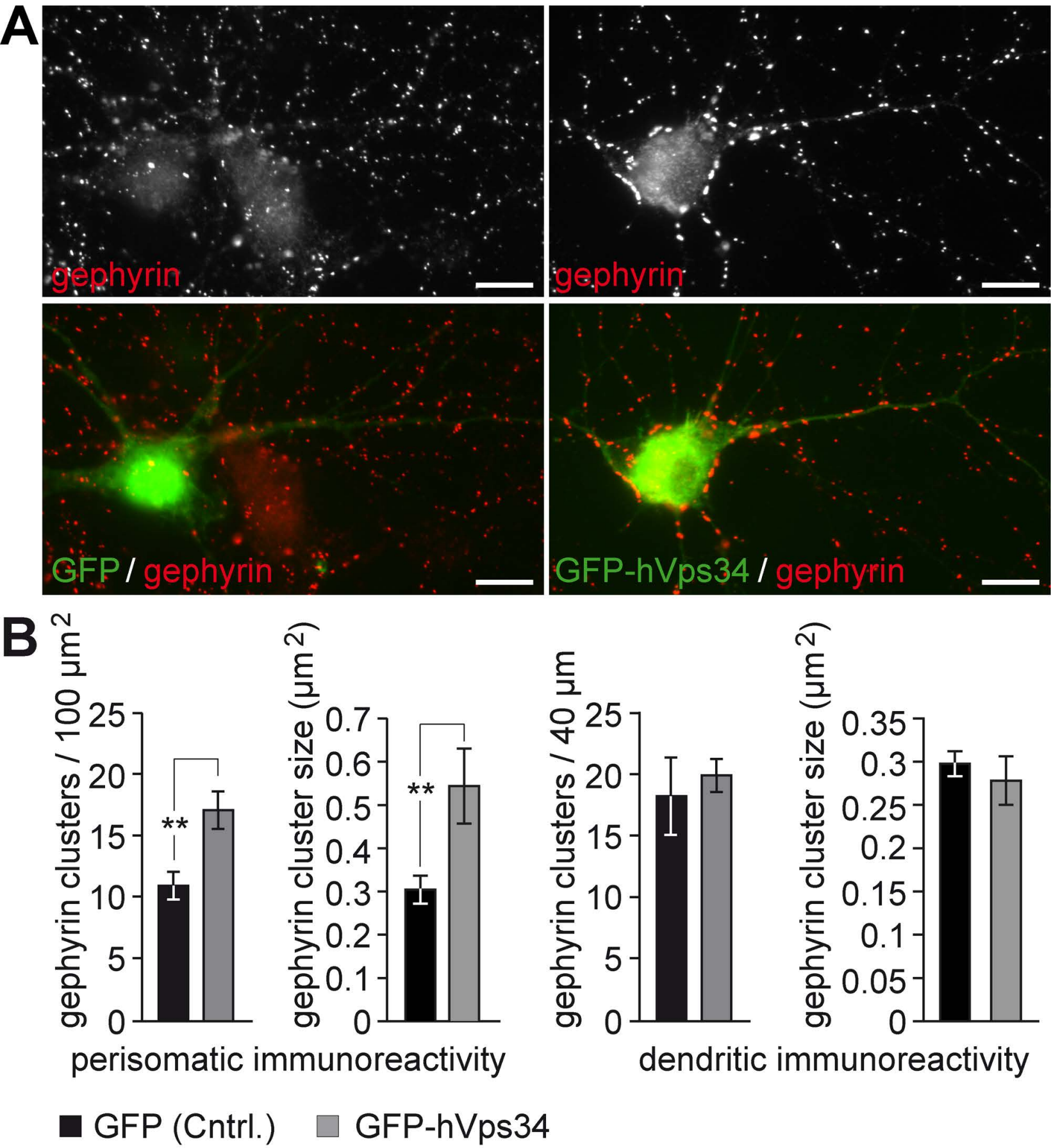
A
gephyrin
gephyrin
GFP / gephyrin
GFP-hVps34 / gephyrin
B
gephyrin clusters / 100 µm2
gephyrin cluster size (µm2)
gephyrin clusters / 40 µm
gephyrin cluster size (µm2)
**
**
perisomatic immunoreactivity
dendritic immunoreactivity
GFP (Cntrl.)
GFP-hVps34

FIGURE 9

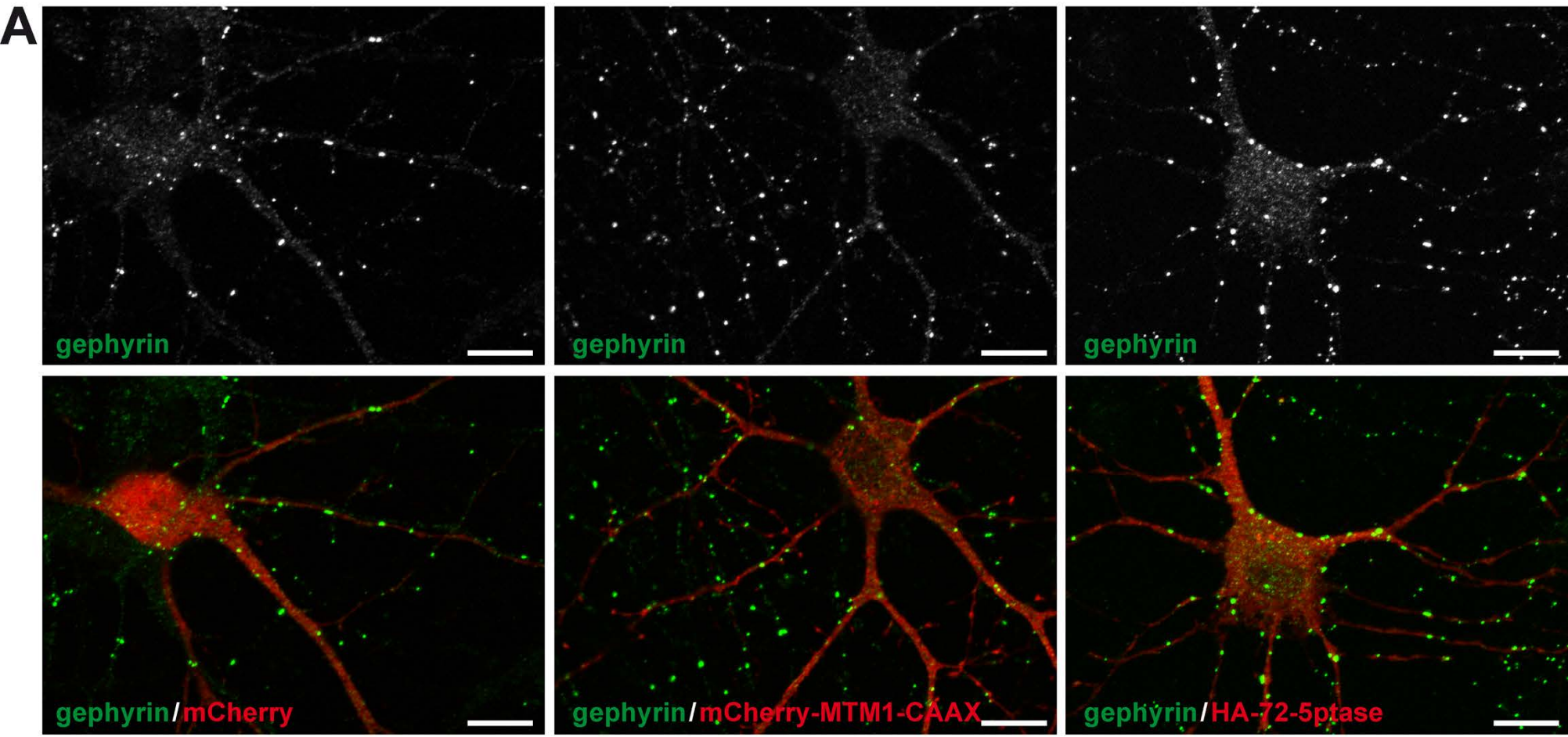
A
gephyrin
gephyrin
gephyrin
gephyrin/mCherry
gephyrin/mCherry-MTM1-CAAX
gephyrin/HA-72-5ptase

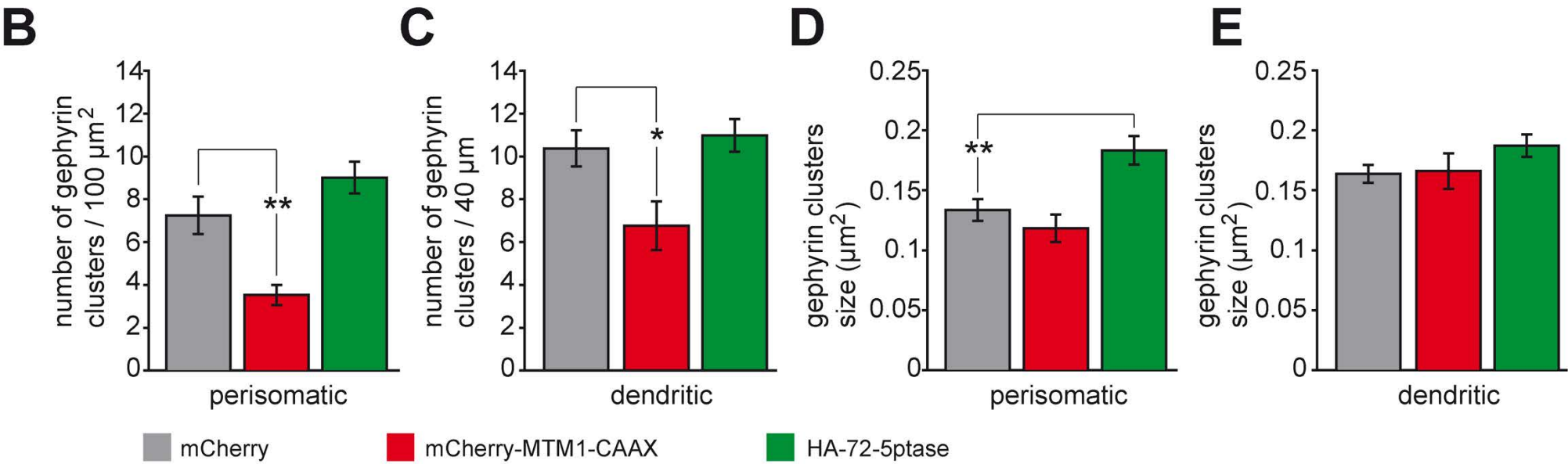
B
number of gephyrin clusters / 100 µm2
14
12
10
8
6
4
2
0
**
perisomatic
C
number of gephyrin clusters / 40 µm
14
12
10
8
6
4
2
0
*
dendritic
D
gephyrin clusters size (µm2)
0.25
0.2
0.15
0.1
0.05
0
**
perisomatic
E
gephyrin clusters size (µm2)
0.25
0.2
0.15
0.1
0.05
0
dendritic
mCherry
mCherry-MTM1-CAAX
HA-72-5ptase

FIGURE 10

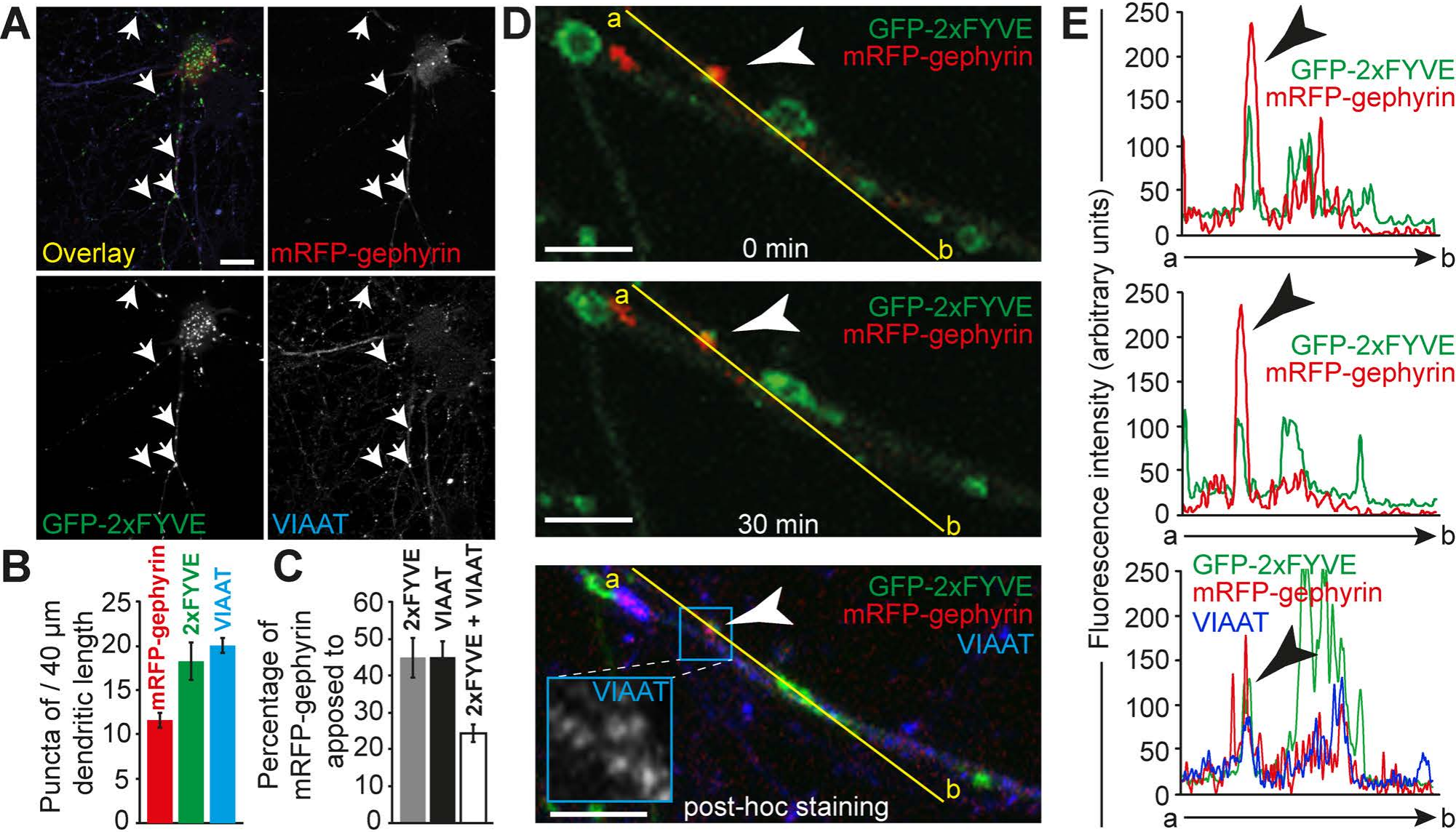
A
Overlay
mRFP-gephyrin
GFP-2xFYVE
VIAAT
B
Puncta of / 40 µm dendritic length
mRFP-gephyrin
2xFYVE
VIAAT
C
Percentage of mRFP-gephyrin apposed to
2xFYVE
VIAAT
2xFYVE + VIAAT
D
a
b
GFP-2xFYVE
mRFP-gephyrin
0 min
30 min
VIAAT
post-hoc staining
E
Fluorescence intensity (arbitrary units)
GFP-2xFYVE
mRFP-gephyrin
VIAAT

FIGURE 11

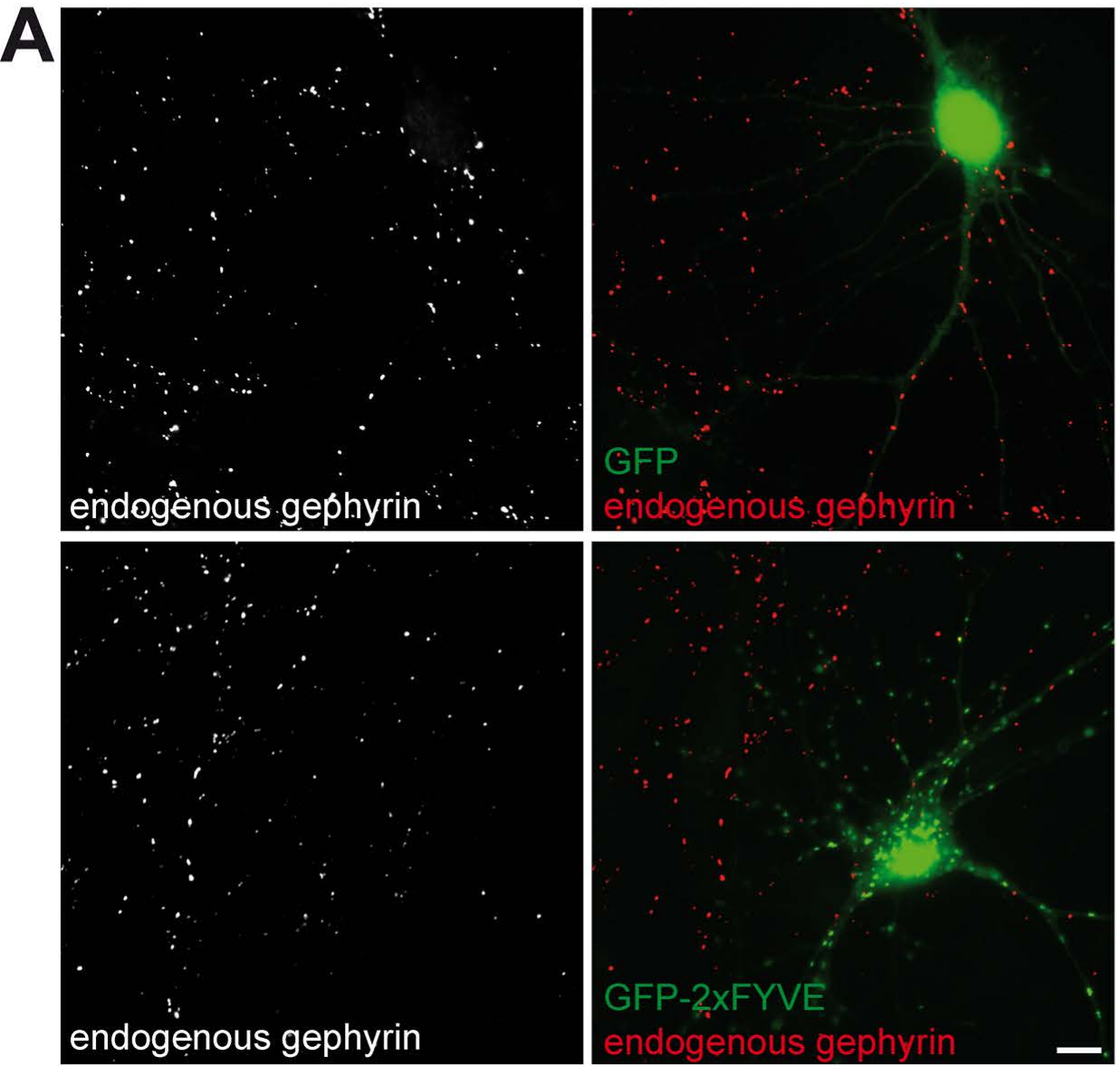
A
endogenous gephyrin
GFP
endogenous gephyrin
endogenous gephyrin
GFP-2xFYVE
endogenous gephyrin

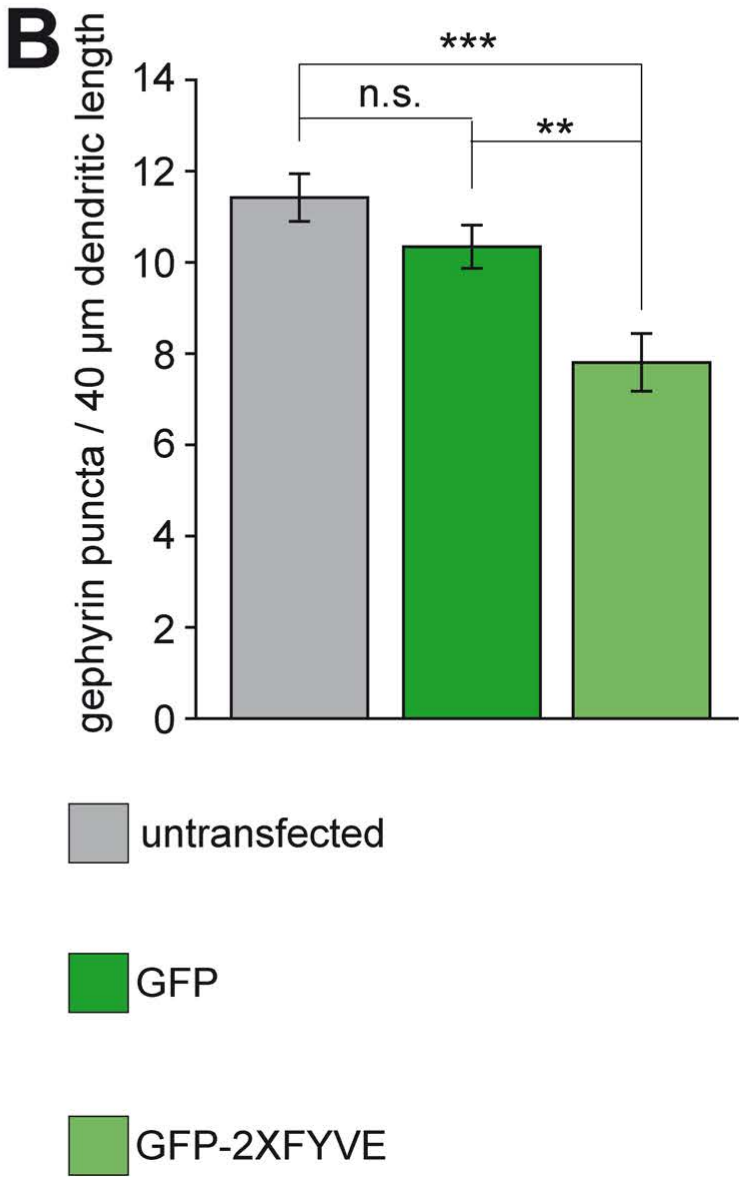
B
gephyrin puncta / 40 µm dendritic length
0
2
4
6
8
10
12
14
***
n.s.
**
untransfected
GFP
GFP-2XFYVE

FIGURE 12

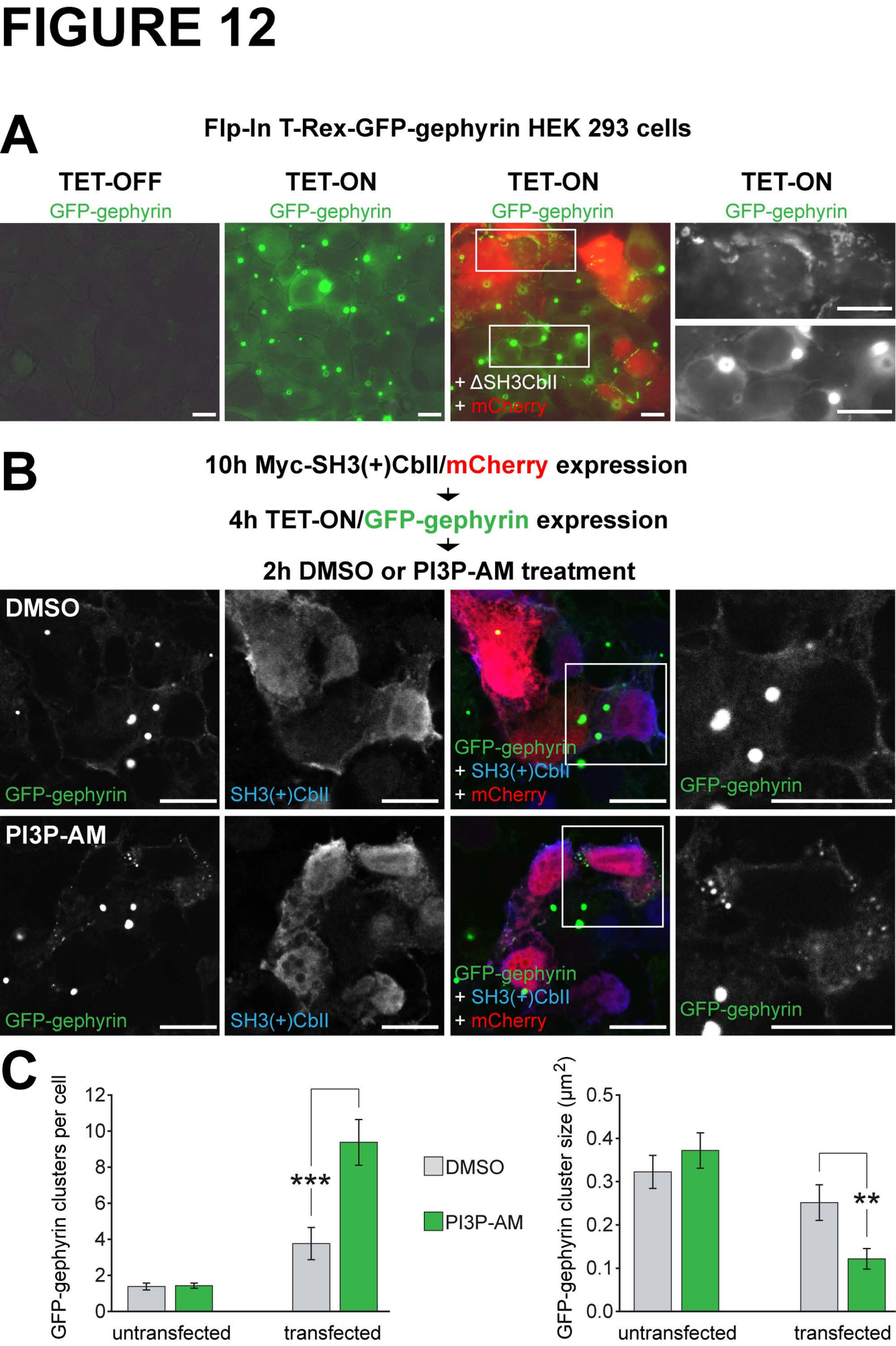
A
Flp-In T-Rex-GFP-gephyrin HEK 293 cells
TET-OFF
GFP-gephyrin
TET-ON
GFP-gephyrin
TET-ON
GFP-gephyrin
+ ΔSH3CblI
+ mCherry
TET-ON
GFP-gephyrin
B
10h Myc-SH3(+)CblI/mCherry expression
4h TET-ON/GFP-gephyrin expression
2h DMSO or PI3P-AM treatment
DMSO
GFP-gephyrin
SH3(+)CblI
GFP-gephyrin
+ SH3(+)CblI
+ mCherry
GFP-gephyrin
PI3P-AM
GFP-gephyrin
SH3(+)CblI
GFP-gephyrin
+ SH3(+)CblI
+ mCherry
GFP-gephyrin
C
GFP-gephyrin clusters per cell
12
10
8
6
4
2
0
***
untransfected
transfected
DMSO
PI3P-AM
GFP-gephyrin cluster size (μm2)
0.5
0.4
0.3
0.2
0.1
0.0
**
untransfected
transfected

FIGURE 13

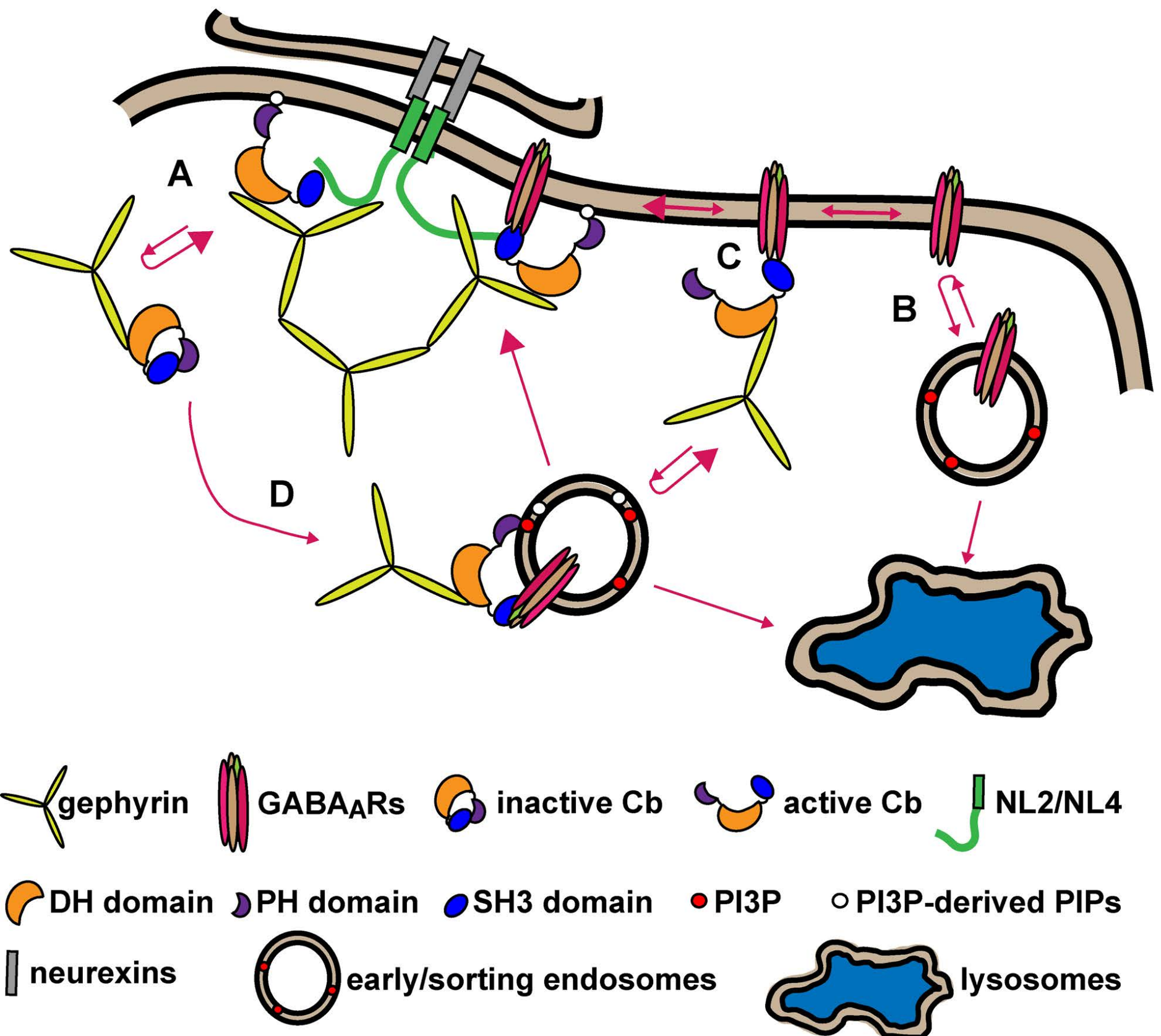
A
B
C
D
gephyrin
GABA$_A$Rs
inactive Cb
active Cb
NL2/NL4
DH domain
PH domain
SH3 domain
PI3P
PI3P-derived PIPs
neurexins
early/sorting endosomes
lysosomes

Endosomal Phosphatidylinositol-3-Phosphate Promotes Gephyrin Clustering and GABAergic Neurotransmission at Inhibitory Postsynapses

Theofilos Papadopoulos, Hong Jun Rhee, Devaraj Subramanian, Foteini Paraskevopoulou, Rainer Mueller, Carsten Schultz, Nils Brose, Jeong-Seop Rhee and Heinrich Betz

J. Biol. Chem. published online December 9, 2016
